5/5-2-96

DOE/ER/14380--T1

HUGHES

SPACE AND COMMUNICATIONS

A HUGHES ELECTRONICS COMPANY

FINAL REPORT

ADVANCED NICKEL-METAL HYDRIDE CELL DEVELOPMENT

GRANT NUMBER DE-FG03-93ER14380

(September 1993 to March 1996)

HUGHES SPACE & COMMUNICATIONS COMPANY

Torrance, California

(prepared by Hong S. Lim)

March, 1996

Prepared for

DEPARTMENT OF ENERGY

Washington, DC 20585

FINAL REPORT

ADVANCED NICKEL-METAL HYDRIDE CELL DEVELOPMENT

GRANT NUMBER DE-FG03-93ER14380
(September 1993 to March 1996)

HUGHES SPACE & COMMUNICATIONS COMPANY
Torrance, California
(prepared by Hong S. Lim)

March, 1996

Prepared for
DEPARTMENT OF ENERGY
Washington, DC 20585

TABLE OF CONTENTS

EXECUTIVE SUMMARY

A nickel-metal hydride (Ni/MH_x) cell is a storage battery cell which is rapidly emerging in recent years for many applications, especially for consumer electronics. A Ni/MH_x cell is an alkaline storage cell similar in many aspects to a nickel-cadmium (Ni/Cd) cell which has been the main workhorse for many electronic devices. The Ni/MH_x system has recently received a special attention from many battery developers and manufacturers especially due to environmental safety concerns regarding the Ni/Cd cell, while general demands for a reliable portable power sources are ever increasing. Concerns on toxicity of cadmium have lead to stricter government environmental regulations both in production processes and disposal of cells. Such regulations made it more difficult to manufacture Ni/Cd cells and dispose of them economically after use. The Ni/MH_x cell has higher gravimetric and volumetric energy densities than Ni/Cd cells by approximately 30%. The Ni/MH_x cell has also the advantage of being able to replace a Ni/Cd cell virtually without a change of the existing power systems for many electronic devices because it is similar to a Ni/Cd cell in physical structure as well as in the charge and discharge voltage characteristics. Although Ni/MH_x cells are now available from several battery manufacturers, further improvements of the cell are desired for long cycle life, low self-discharge, and operation at elevated temperatures. Performance of the cell for these characteristics are closely related to the alloy properties. Therefore, it is highly desirable to improve the hydride alloy material for an improved Ni/MH_x cell. Preparation technique and alloy composition affect the performance. The most popular preparation technique of the alloy powder is pulverization on an ingot prepared by arc- or induction-melting. It has been reported that an alloy prepared by a rapid cooling technique resulting in small grain, columnar structure give longer cycle life than a large grain, equiaxed structure from a slow cooling technique. An atomization technique of a molten alloy will be a logical technique for rapid-cooling of the alloy.

For an effort to develop an advance Ni/MH_x cell, this research was directed at developing a new preparation technique of alloy material for use as anodes of Ni/MH_x cells. This was a collaborative effort of four organizations which include Texas A&M University (TAMU), Brookhaven National Laboratory (BNL), Los Alamos National Laboratory (LANL), and Hughes. We have studied four different alloy preparation techniques. These techniques are pulverization of arc- or induction-melted ingots, ball-milling, and atomization techniques. Arc-melting technique was studied at BNL, ball-milling at LANL, and the pulverization and atomization techniques at Hughes. TAMU studied basic scientific properties of the alloy powders.

We, at Hughes, have studied inert gas atomization technique for a potential production method of the alloy powder using several metal hydride alloys which are attractive for a Ni/MH_x cell. Atomization of the alloys was demonstrated successfully in a small production quantity (up to a batch-size of several kilograms). The relative performance of the atomized and corresponding non-atomized alloys were investigated for the electrode material in a Ni/MH_x cell. The study included effects of charge-discharge rates, temperature, and particle size on cell voltage (polarization) and specific capacity. Results show that the specific capacity of the present atomized alloys was appreciably smaller than the corresponding non-atomized powder, especially for initial cycles. Full activation of the atomized alloys often took several hundreds of cycles. Even after full activation, the specific capacity of the atomized alloys was smaller than that of the corresponding non-atomized alloy. However, no appreciable difference in discharge rate capability was observed with some alloys. Results of chemical analyses of the metallic composition were indistinguishable between the atomized and non-atomized alloys. However, the oxygen contents of the atomized alloys were always higher, by a factor of 3 or more, than those of the non-atomized alloys. We suspect that the high oxygen content might be a factor for the low specific capacity of the atomized alloys. We have also studied the effect of annealing of the atomized alloys at 1100°C, since we suspected that a lack of crystallinity might be another factor for the low specific capacity of the atomized alloys. The annealing improved the capacity, but the alloy capacity is still smaller than that of the non-atomized alloy.

Effects of Ni- and Cu coating on the alloy performance were studied after coating the powder alloys using an electroless coating technique. Coatings of both metals noticeably improved the electrode rate capability for all alloy samples studied. Especially, the improvement in the electrode polarization for atomized alloys was tremendous. However, the coating did not appear to improve their cycle life. Spherical geometry of the atomized powder allowed us a means of direct observation of the mechanism and rate of physical changes of the alloy particles. Present results of a preliminary investigation are not conclusive in determining the possible merits of the atomization technique, even though overall performance of the non-atomized alloy was superior to that of the atomized alloy. Further studies are needed, especially to reduce the oxygen contents in the atomized alloys, to explore possible merits of atomization technique, e.g., possible improved life without sacrificing the specific capacity and the rate capability.

1. INTRODUCTION

A nickel-metal hydride (Ni/MH_x) cell is a storage battery cell which is rapidly emerging in recent years for many applications especially, for consumer electronics. A Ni/MH_x cell is an alkaline storage cell and is similar in many aspects to a nickel-cadmium (Ni/Cd) cell, which has been the main workhorse for many electronic devices. The Ni/MH_x system has recently received a special attention from many battery developers and manufacturers especially due to environmental safety concerns regarding the Ni/Cd cell, while general demands for a reliable portable power sources are ever increasing. Concerns on toxicity of cadmium have lead to stricter government environmental regulations both in production processes and disposal of the cells. Such regulations made it more difficult to manufacture Ni/Cd cells and dispose of them economically after use. For most applications a storage cell is generally preferred to a primary cell due to the disposal problem. The Ni/MH_x cell has higher gravimetric and volumetric energy densities than Ni/Cd cells by approximately 30%. The Ni/MH_x cell has also the advantage of being able to replace a Ni/Cd cell virtually without a change of the existing power systems for many electronic devices because they are similar in physical structure as well as in the charge and discharge voltage characteristics.

Ni/MH_x cells are now available from several battery manufacturers. However, further improvements of the cell are desired for long cycle life, low self-discharge, and operation at an elevated temperature. Performance of the cell for these characteristics are closely related to the alloy properties. Therefore, it is highly desirable to improve the hydride alloy material for an improved Ni/MH_x cell. Preparation technique of the alloys as well as its composition has been reported to affect the performance (1, 2). Most popular preparation techniques of the alloy powder are an arc-melting and melting in an induction furnace followed by a mechanical pulverization. However, such melting techniques have disadvantage in keeping a low boiling metal from loosing by evaporation for alloys which contain a low boiling metal such as magnesium or calcium. For these alloys a mechanical alloying (ball-milling) (3, 4, 5) will be preferable. It has also been reported that an AB_5-type alloy prepared by a rapid cooling technique resulting in small grain (approximately 10 μm) columnar structure give longer cycle life than an equiaxed, large grain (approximately 50 μm) structure from a slow cooling technique (6). An atomization technique of a molten alloy (7, 8) will be a logically preferred technique for a rapid-cooled alloy.

For an initial effort to develop an advance Ni/MH_x cell (9,10), this research is directed at developing a new preparation technique of alloy material for use as anodes in nickel-metal hydride cells. This is a collaborative effort of four organizations which include Texas A&M University (TAMU), Brookhaven National Laboratory (BNL), Los Alamos National Laboratory (LANL), and Hughes. We have studied four different alloy preparation techniques. These techniques are pulverization of arc- or induction-melted ingots, mechanical alloying (ball-milling), and atomization techniques. Arc-melting technique was studied at BNL, mechanical alloying at LANL, and the pulverization and atomization techniques at Hughes. TAMU carried out basic scientific investigations of the alloy powder prepared by these techniques. We also investigated other practical methods of improving the performance of the metal hydride anode at Hughes. We have studied the effects of nickel and copper surface coatings of alloy particles on the MH_x electrode performance. It has been reported that such coatings improve rate capability, utilization, and cycle life performance (11, 12, 13). The present report describes results obtained at Hughes.

2. HYDRIDE ALLOYS

The hydride alloys studied in this report and their preparation techniques are shown in Table 1. The compositions were selected based on the results of our previous study (14) after a careful review of available results at the time of the selection. The basis of the selection was technical performance of the alloys, especially high specific capacity and long cycle life capability. All induction melting and atomization runs were carried out at Retech, Inc., Ukiah, CA, unless otherwise specified. "Mechanical powder" was prepared by breaking alloy ingots using a stainless steel mortar followed by sieving in a nitrogen filled glove box. Elemental analyses of the alloys were carried out by dc plasma analysis technique at either Metallurgical Testing Corporation, City of Industry, CA, or Wah Chang Albany Analytical Services, Albany, OR. Results of the elemental analyses are shown in Tables 2 to 5.

Table 1. Compositions of the alloys studied in this work.

Sample ID	Compositions	Preparation Technique
E931*	$La_{0.8}Ce_{0.2}Ni_{4.75}Sn_{0.25}$	Induction melt./mechanical powder
E931*	$La_{0.8}Ce_{0.2}Ni_{4.75}Sn_{0.25}$	Induction melt./atomization
E932*	$La_{0.8}Ce_{0.2}Ni_{3.75}Co_{1.0}Sn_{0.25}$	Induction melt./mechanical powder
E932*	$La_{0.8}Ce_{0.2}Ni_{3.75}Co_{1.0}Sn_{0.25}$	Induction melt./atomization
R01	$La_{0.5}Ce_{0.5}Ni_{3.55}Co_{0.75}Mn_{0.4}Al_{0.3}$	He-arc melting/atomization
R02	$La_{0.8}Ce_{0.2}Ni_{3.55}Co_{0.75}Mn_{0.4}Al_{0.3}$	He-arc melting/atomization
R03	$La_{0.5}Ce_{0.5}Ni_{3.55}Co_{0.75}Mn_{0.4}Sn_{0.3}$	He-arc melting/atomization
R04	$La_{0.5}Ce_{0.5}Ni_{3.55}Co_{0.75}Mn_{0.4}Al_{0.3}Sn_{0.2}$	He-arc melting/atomization
R05	$La_{0.7}Ce_{0.3}Ni_{3.2}Co_{1.0}Mn_{0.6}Al_{0.2}$	He-arc melting/atomization
R06	$La_{0.7}Ce_{0.3}Ni_{3.2}Co_{1.0}Mn_{0.6}Al_{0.2}$	He-arc melting/atomization
R07	$La_{0.6}Ce_{0.3}Zr_{0.1}Ni_{3.2}Co_{1.0}Mn_{0.6}Al_{0.2}$	He-arc melting/atomization
R08	$La_{0.5}Ce_{0.3}Ca_{0.2}Ni_{3.2}Co_{1.0}Mn_{0.6}Al_{0.2}$	He-arc melting/atomization
R09	$La_{0.7}Ce_{0.3}Ni_{3.3}Co_{1.0}Mn_{0.4}Al_{0.3}$	He-arc melting/mechanical powder
R10-1	$La_{0.7}Ce_{0.3}Ni_{3.2}Co_{1.0}Mn_{0.6}Al_{0.2}$	He-arc melting/atomization**
R10-2	$La_{0.7}Ce_{0.3}Ni_{3.2}Co_{1.0}Mn_{0.6}Al_{0.2}$	He-arc melting/mechanical powder
R11	$La_{0.6}Ce_{0.3}Zr_{0.1}Ni_{3.2}Co_{1.0}Mn_{0.6}Al_{0.2}$	He-arc melting/mechanical powder
R12	$La_{0.7}Ce_{0.3}Ni_{3.3}Co_{1.0}Mn_{0.4}Al_{0.3}$	He-arc melting/atomization**
R13	$La_{0.7}Ce_{0.3}Ni_{3.2}Co_{1.0}Mn_{0.6}Al_{0.2}$	He-arc melting/atomization

* Prepared at Ergenics, Inc., Ringwood, N.J. 07456.
** Atomized at Crucible Materials, Pittsburgh, PA.

Table 2. Results of elemental analyses of atomized alloys R01 through R05 and alloy button before the atomization.

		R01	R02	R03	R04	R05-1	R05-2	R05 Block
La, Wt%	calc.	16.45	26.34	15.44	16	22.91	22.91	22.91
	anal.	16.88	25.94	15.99	17.33	22.3	22.12	25.27
	delta	0.4	-0.4	0.5	1.3	-0.6	-0.8	2.4
Ce, Wt%	calc.	16.59	6.64	15.58	16.14	9.9	9.9	9.9
	anal.	17.62	7.65	16.66	16.97	10.78	10.46	12.89
	delta	1	1	1.1	0.8	0.9	0.6	3
Ni, Wt%	calc.	49.36	49.41	46.34	45.3	44.26	44.26	44.26
	anal.	48.8	49.8	46.9	42.5	45.1	45.1	41.6
	delta	-0.6	0.4	0.6	-2.8	0.8	0.8	-2.7
Co, Wt%	calc.	10.47	10.48	9.83	10.18	13.88	13.88	13.88
	anal.	10.23	10.16	9.64	10.47	13.49	13.99	12.43
	delta	-0.2	-0.3	-0.2	0.3	-0.4	0.1	-1.5
Mn, Wt%	calc.	5.2	5.21	4.89	5.06	7.77	7.77	7.77
	anal.	4.79	4.82	4.28	5.38	6.92	7.02	6.75
	delta	-0.4	-0.4	-0.6	0.3	-0.8	-0.7	-1
Al, Wt%	calc.	1.92	1.92		1.86	1.27	1.27	1.27
	anal.	1.54	1.56		1.59	1.02	1.11	0.97
	delta	-0.4	-0.4		-0.3	-0.3	-0.2	-0.3
Sn, Wt%	calc.			7.92	5.47			
	anal.			6.35	5.73			
	delta			-1.6	0.3			

Table 3. Results of elemental analyses of atomized and button alloys of R06, R07 and R08.

		R06 Atomized	R06 Button	R07 Atomized	R07 Button	R08 Atomized	R08 Button
La, Wt%	calc.	22.91	22.91	19.86	19.86	17.16	17.16
	anal.	21.5	21.3	18.54	18.87	15.81	17
	delta	-1.4	-1.6	-1.3	-1	-1.4	-0.2
Ce, Wt%	calc.	9.9	9.9	10.02	10.02	10.39	10.39
	anal.	11.07	10.45	10.81	11.08	11.16	11.6
	delta	1.2	0.5	0.8	1.1	0.8	1.2
Ni, Wt%	calc.	44.26	44.26	44.77	44.77	46.43	46.43
	anal.	45.5	46.5	46.8	45.8	49.9	48.3
	delta	1.2	2.2	2	1	3.5	1.9
Co, Wt%	calc.	13.88	13.88	14.04	14.04	14.56	14.56
	anal.	13.54	13.3	13.39	13.52	13.5	14.24
	delta	-0.3	-0.6	-0.7	-0.5	-1.1	-0.3
Mn, Wt%	calc.	7.77	7.77	7.85	7.85	8.15	8.15
	anal.	7.05	7.19	7.15	7.18	7	7.48
	delta	-0.7	-0.6	-0.7	-0.7	-1.1	-0.7
Al, Wt%	calc.	1.27	1.27	1.29	1.29	1.33	1.33
	anal.	1.06	1.08	1.03	1.07	1.17	1.07
	delta	-0.2	-0.2	-0.3	-0.2	-0.2	-0.3
Zr, Wt%	calc.			2.17	2.17		
	anal.			2.09	2.34		
	delta			-0.1	0.2		
Ca, Wt%	calc.					1.98	1.98
	anal.					0.18	0.15
	delta					-1.8	-1.8

Table 4. Results of elemental analyses of atomized and button alloys including oxygen content.

		R06* Atomized	R07* Atomized	R07# Atomized	R09# Button	R10# Button	R11# Button
La, Wt%	calc.	22.91	19.86	19.86	23.04	22.91	21.39
	anal.	21.50	18.54	19.20	22.20	22.20	20.10
	delta	-1.40	-1.30	-0.70	-0.80	-0.70	-1.30
Ce, Wt%	calc.	9.90	10.02	10.02	9.96	9.90	9.96
	anal.	11.07	10.81	9.10	8.59	9.04	9.37
	delta	1.20	0.80	-0.90	-1.40	-0.90	-0.60
Ni, Wt%	calc.	44.26	44.77	44.77	45.91	44.26	44.51
	anal.	45.50	46.80	46.00	47.00	45.30	46.40
	delta	1.20	2.00	1.20	1.10	1.00	1.90
Co, Wt%	calc.	13.88	14.04	14.04	13.96	13.88	13.96
	anal.	13.54	13.39	14.40	14.90	14.50	14.00
	delta	-0.30	-0.70	0.40	0.90	0.60	0.00
Mn, Wt%	calc.	7.77	7.85	7.85	5.21	7.77	7.81
	anal.	7.05	7.15	7.80	5.25	7.60	7.62
	delta	-0.70	-0.70	-0.10	0.00	-0.20	-0.20
Al, Wt%	calc.	1.27	1.29	1.29	1.92	1.27	1.28
	anal.	1.06	1.03	1.38	2.04	1.36	1.40
	delta	-0.20	-0.30	0.10	0.10	0.10	0.10
Zr, Wt%	calc.		2.17	2.17			1.08
	anal.		2.09	1.86			0.96
	delta		-0.10	-0.30			-0.10
O, Wt%	calc.	0.00	0.00	0.00	0.00	0.00	0.00
	anal.	0.33	0.20	0.24	0.02	0.01	0.01
	delta	0.30	0.20	0.24	0.02	0.01	0.01

* Metallugical Testing Corp. #Wah Chang Albany Analytical Services.

Table 5. Results of elemental analyses of atomized (at C.M.) and button alloys including oxygen content.

		R10* Atomized	R12* Atomized	R13* Atomized	R10# Atomized	R12# Button	R13# Button
La, Wt%	calc.				22.91	23.04	22.91
	anal.				21.80	22.80	22.70
	delta				-0.11	-0.24	-0.21
Ce, Wt%	calc.				9.90	9.96	9.90
	anal.				9.80	9.72	9.85
	delta				-0.10	-0.24	-0.05
Ni, Wt%	calc.				44.26	45.91	44.26
	anal.				46.00	46.40	44.80
	delta				1.74	0.49	0.54
Co, Wt%	calc.				13.88	13.96	13.88
	anal.				14.10	14.30	14.20
	delta				0.22	0.34	0.32
Mn, Wt%	calc.				7.77	5.21	7.77
	anal.				7.09	4.81	7.24
	delta				-0.68	-0.40	-0.53
Al, Wt%	calc.				1.27	1.92	1.27
	anal.				1.26	1.94	1.26
	delta				0.01	0.02	0.01
O, Wt%	anal.	0.0269	0.0220	0.0248			
C, Wt%	anal.	0.052	0.035	0.070			
N, Wt%	anal.	0.006	0.004	0.004			

* C.M. #Wah Chang Albany Analytical Services.

3. ATOMIZATION

The basic scheme of the atomization technique is shown in Fig. 1. Atomization was carried out in a water-cooled copper crucible by passing molten alloy through an orifice in an inert atmosphere (He or Ar) while an inert gas jet is directed to the molten stream of the alloy. The size of orifice was 0.94 to 1.25 cm in diameter. The inert gas nozzle was approximately 0.2 cm in inner diameter. The inert atmosphere chamber at near atmospheric pressure typically contained 4~10 ppm of oxygen and approximately 30 ppm of H_2O. The He gas for the atomization runs contained typically 2.5 ppm of oxygen and approximately 8 ppm of H_2O. The source gas pressure varied from 100 to 400 psi. Batch size for the atomization was typically 3 to 5 kg. Resulting alloy powders with various particle size were collected and sieved through sieves of various sizes. Typical test samples were in the particle size range of 38-90 μm (-170+400 mesh) unless otherwise specified. Scanning electron microscope (SEM) picture of typical atomized powder is shown in Fig. 2. Particle size distributions of the alloys for typical atomization runs are shown in Fig 3. Test runs were for demonstration of the atomization in a small production scale and to prepare test samples for MH_x electrodes. Therefore, the atomization conditions were not optimized for maximum yield of certain particle size fractions.

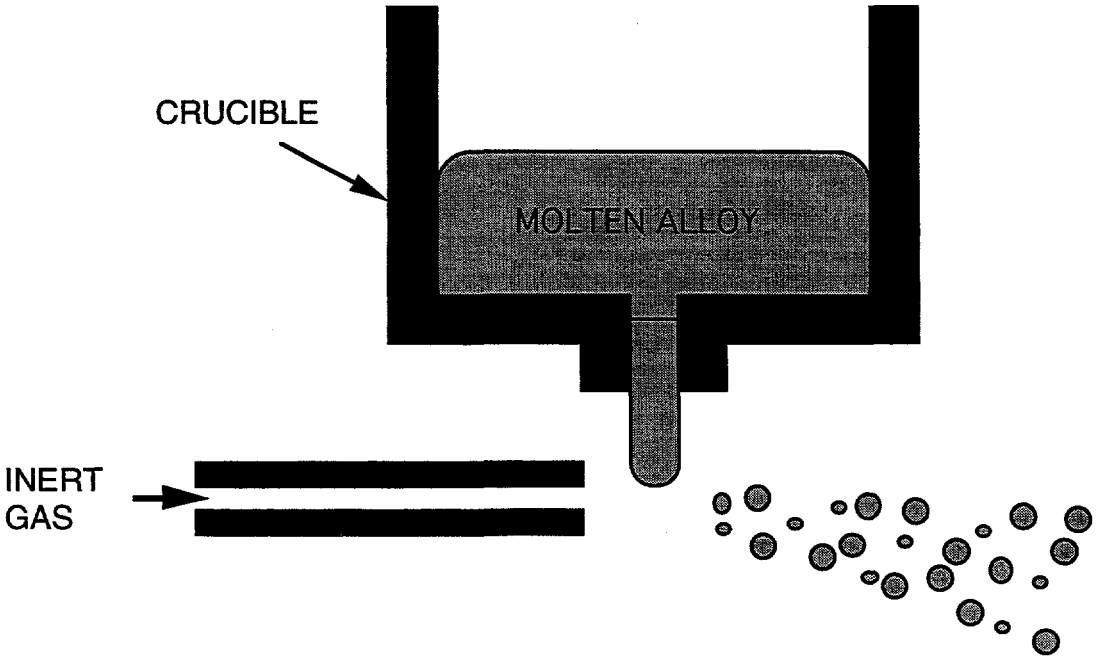

Fig. 1. A schematic drawing of atomization technique.

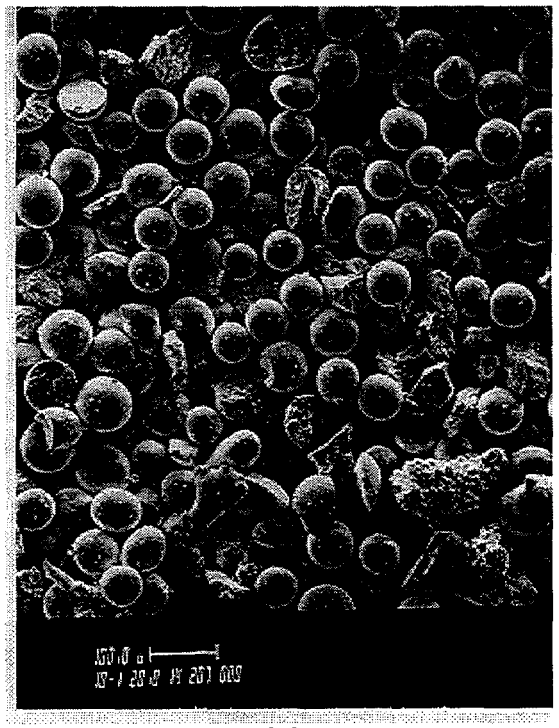

(a)

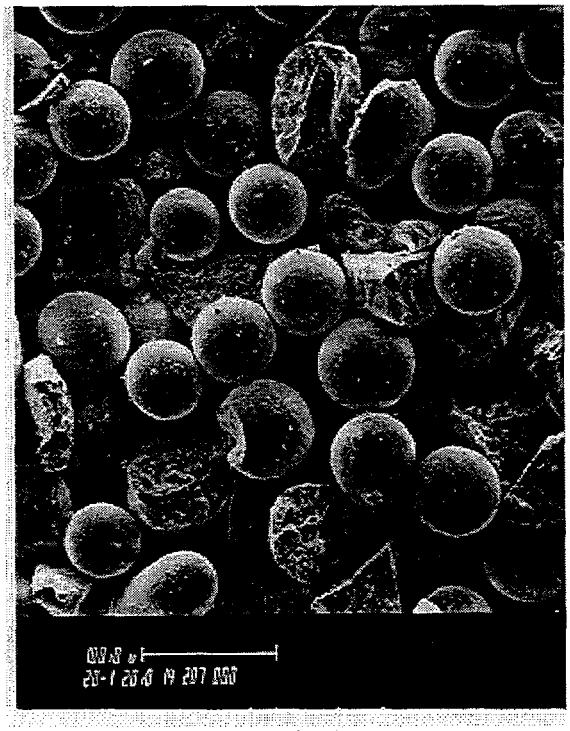

(b)

Fig. 2. SEM photograph of -170+230 mesh size fraction (63-90 μm) of the atomized powder of R01 alloy. (a): 100x. (b): 200x. (c): 500x.

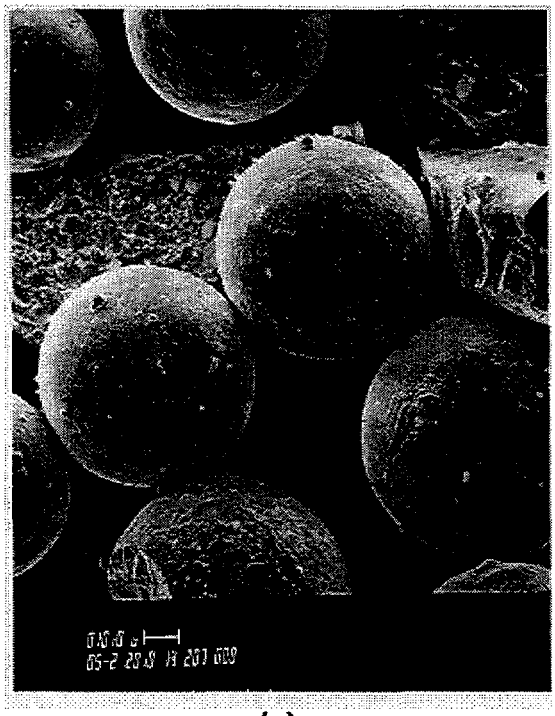

(c)

Fig. 2. Continued.

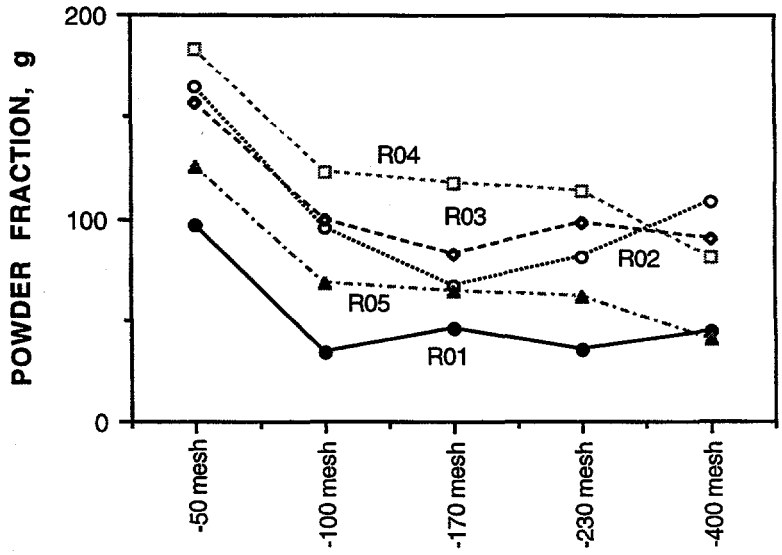

Fig. 3. Distribution powder size fractions of typical atomization runs.

4. TEST CELLS AND CYCLE REGIMES

Test Electrodes and Cells -- The metal hydride (MH_x) electrodes for evaluation of the alloys were prepared by pasting a slurry of the alloy powder, Shawinigan acetylene black (AB50), and polybenzimidazole (PBI) solution on a piece of nickel foam substrate of 80 to 100 pores per inch. Test electrodes were approximately 2.3 cm x 2.3 cm in size. Each electrode contained approximately 1 g of alloy. Performance tests of the MH_x electrodes are carried out in a flooded electrolyte Ni/MH_x cell shown in Fig. 4. Test cells were activated by addition of 31% KOH (by weight) electrolyte followed immediately by trickle charging at 10 to 20 mA to prevent possible corrosive oxidation of the active alloy material for a minimum of several hours before measuring their initial capacities.

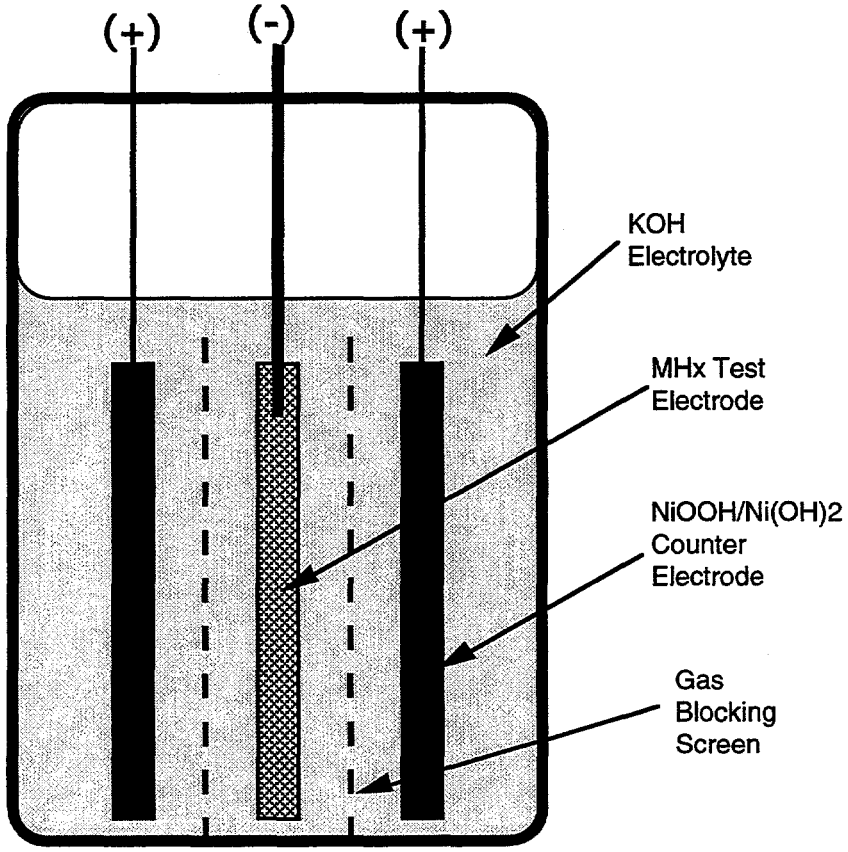

Fig. 4. A schematic drawing of flooded electrolyte Ni/MH_x test cell.

Test Cycle Regimes -- Capacity tests were carried out by charging test cells at 165 mA for 2.5 h followed by discharge of the cell at the same rate to 1.0 V. The standard cycling test regime

was an aerospace low earth orbit (LEO) regime at approximately 50% depth-of-discharge with 110% recharge, i.e., 35 min discharge at 0.86 C rate (285 mA) followed by recharge at 0.60 C (198 mA) for 55 min.

5. ALLOY PERFORMANCE

Measured values of the electrochemical capacity of many alloys, especially the atomized ones, increased with cycling indicating that the alloys were not fully activated by a few initial cycles. Some alloys took several hundreds of cycles before they were fully activated as shown in Fig. 5. In this activation period, measured values of the electrode capacity, especially from one electrode to another, were rather irreproducible. It is difficult to make precise comparison of capacities of different alloys due to the slow activation and irreproducibility of the measurements. A rough comparison of maximum specific electrochemical capacities of various alloys is shown in Table 6. The measured specific capacities of atomized powder were much lower, to our surprise, than those of corresponding alloys before atomization especially for those atomized in early period (R01 to R06). Results of elemental analyses of metallic components were indistinguishable between atomized alloys and corresponding non-atomized alloys within an experimental error as shown in Tables 3 and 4. However, oxygen content was much higher in the atomized alloys than in the non-atomized alloys as shown in Tables 4. These results prompted us to have the atomization carried out with another equipment with improved vacuum control for R10, R12 and R13 alloys which showed considerably reduced oxygen contents as shown in Table 5. These alloys also showed significantly improved specific capacities compared with earlier atomized alloys of similar compositions as shown in Table 6. However, those improved values were still lower than those for the corresponding non-atomized alloys. For another step of improvement, the atomized alloys were annealed in a rhenium boat in an inert atmosphere for 72 hours at 1100°C. The annealed powder was sintered together to form a cake. The sintered cake was mechanically broken and sieved to prepare powder of desired particle size. The maximum measured specific capacities of resulting alloys are shown in Table 6. All atomized powders studied showed lower specific capacity than the corresponding non-atomized powder regardless of whether or not it was Ni- or Cu-coated or annealed. Ni- or Cu-coating on atomized powder improved specific capacity probably due to improved kinetics. Annealing of the atomized powder also improved specific capacity.

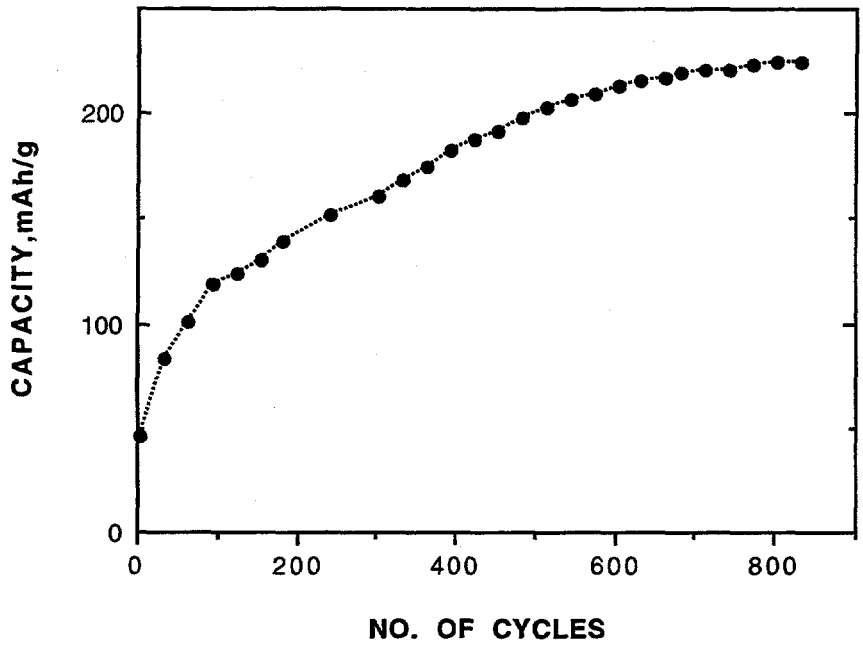

Fig. 5. Capacity change with cycling of a MHx electrode containing atomized powder of R01 alloy in a flooded electrolyte Ni/MH_x cell.

Table 6. A rough comparison of maximum capacities of various alloy.

Sample ID	Max. Measured Capacity, mAh/g	Comments
E931	240	non-atomized
E931	176	atomized
E931	212	atomized, Ni-coated
E932	116	non-atomized
E932	165	atomized
E932	219	atomized, Ni-coated
R01	227	atomized
R01	249	atomized, Ni-coated
R02	226	atomized
R02	257	atomized, Ni-coated
R03	92	atomized
R04	44	atomized
R04	145	atomized, Ni-coated
R05	32	atomized
R05	235	atomized, Ni-coated
R06	329	non-atomized
R06	189	atomized
R06	262	atomized, Cu-coated
R07	280	non-atomized
R07	207	atomized
R08	227	non-atomized
R08	160	atomized
R10	315	non-atomized
R10	190	atomized
R10	268	atomized, annealed
R11	302	non-atomized
R12	321	non-atomized
R12	200	atomized
R12	231	atomized, annealed

Effects of Charge and Discharge Rates and Temperature on Performance -- Discharge voltage curves of test cells containing various non-atomized and atomized alloys were recorded at various rates ranging from approximately 0.2 to 2.0 C rate at temperatures of 2, 10, and 20°C. Results for the non-atomized alloys at 2 and 20°C are shown in Figs. 6 to 11. Results for the atomized alloys are shown in Figs. 12 to 15. Rate capability of alloys at various temperatures are shown in Figs. 16 to 20. Discharge capacity decreased roughly linearly with increase of discharge rate in the studied range with an exception of the non-atomized R12 alloy. Rate capability of various alloys at 20 and 2°C are compared one another in Figs. 21 and 22, respectively. Relative rate capability of alloys were in the decreasing order of R12 $\geq$ R10 > R11 as shown in Figs. 21 and 22 indicating

that a partial substitution of La with Zr cause a reduction in the rate capability. Rate capability of R10 was virtually unchanged by atomization, but that of R12 was decreased by atomization.

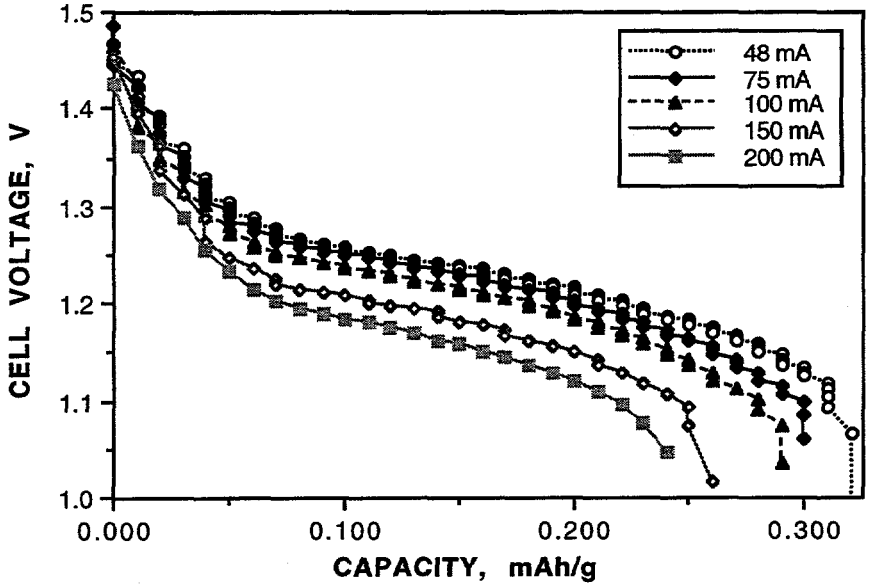

Fig. 6. Effects of discharge rates on cell voltage and capacity at 2°C. Curves are for discharges at various rates (48 to 200 mA) after charging for 165 min at a C/2 rate (120 mA) for a Ni/MH_x cell containing 975 mg of non-atomized R10 alloy powders in size range of 38-53 μm in diameter.

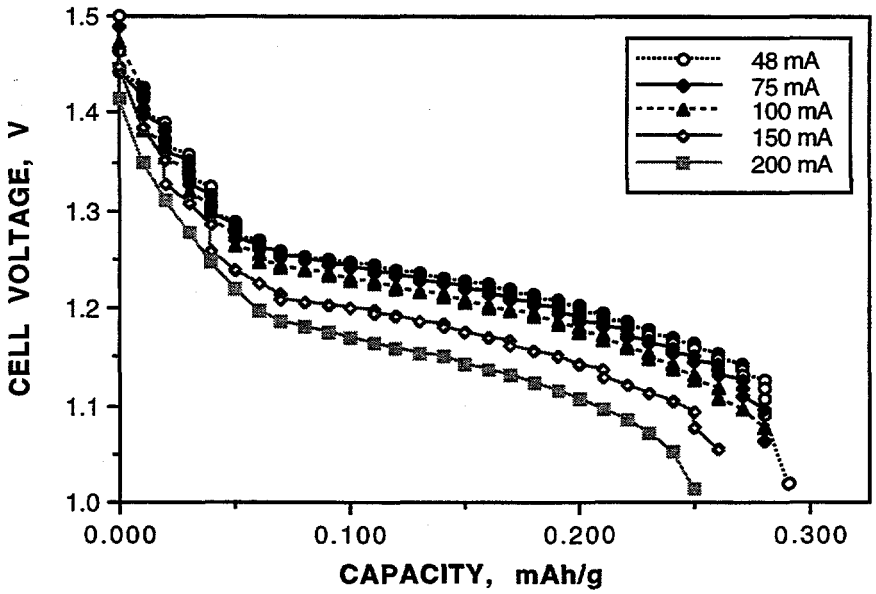

Fig. 7. Effects of discharge rates on cell voltage and capacity at 2°C. Curves are for discharges at various rates (48 to 200 mA) after charging for 165 min at a C/2 rate (120 mA) for a Ni/MH_x cell containing 857 mg of non-atomized R12 alloy powders in size range of 38-53 μm in diameter.

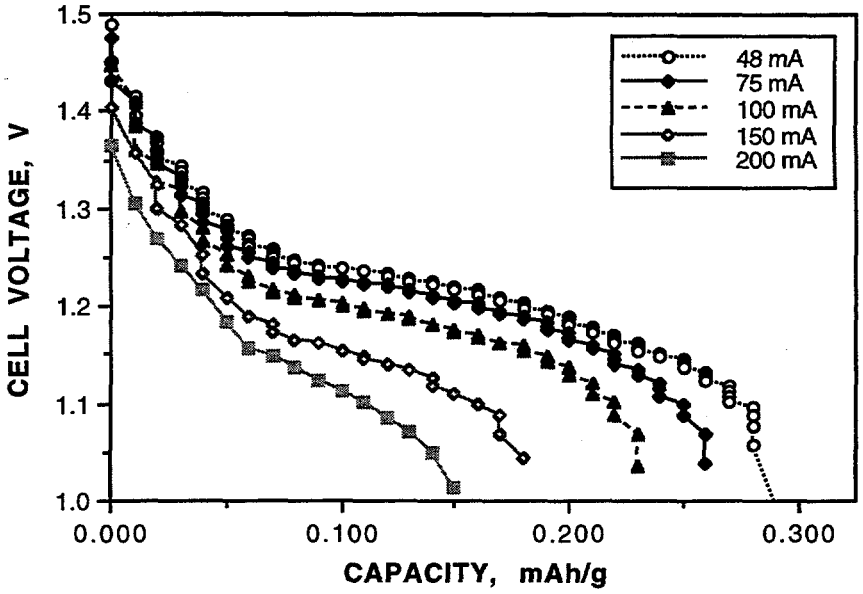

Fig. 8. Effects of discharge rates on cell voltage and capacity at 2°C. Curves are for discharges at various rates (48 to 200 mA) after charging for 165 min at a C/2 rate (120 mA) for a Ni/MH_x cell containing 927 mg of non-atomized R11 alloy powders in size range of 38-53 μm in diameter.

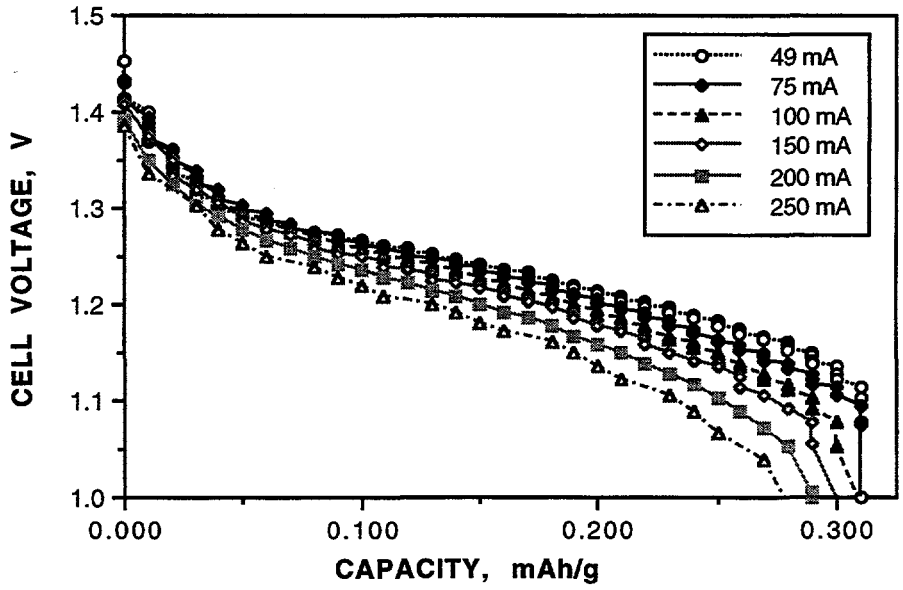

Fig. 9. Effects of discharge rates on cell voltage and capacity at 20°C. Curves are for discharges at various rates (48 to 480 mA) after charging for 165 min at a C/2 rate (120 mA) for a Ni/MH_x cell containing 975 mg of non-atomized R10 alloy powders in size range of 38-53 μm in diameter.

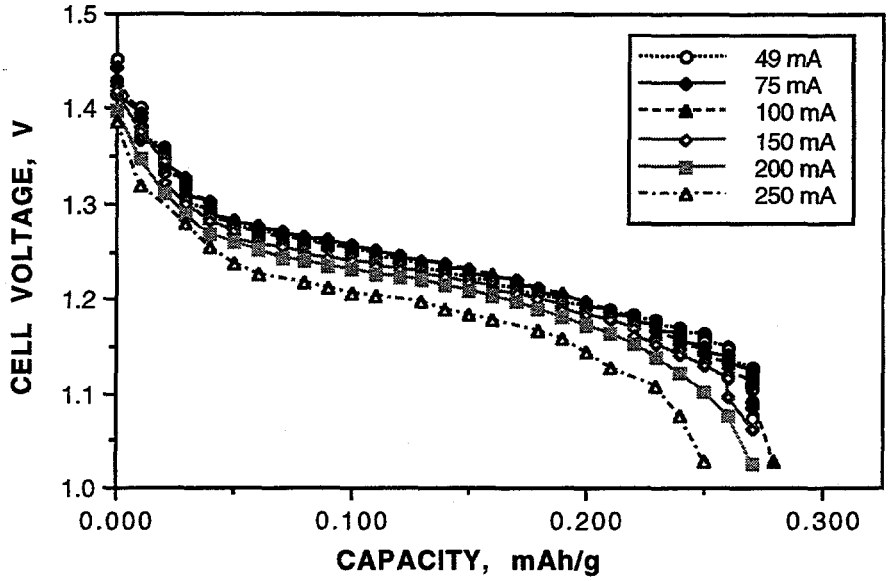

Fig. 10. Effects of discharge rates on cell voltage and capacity at 20°C. Curves are for discharges at various rates (48 to 480 mA) after charging for 165 min at a C/2 rate (120 mA) for a Ni/MH_X cell containing 857 mg of non-atomized R12 alloy powders in size range of 38-53 μm in diameter.

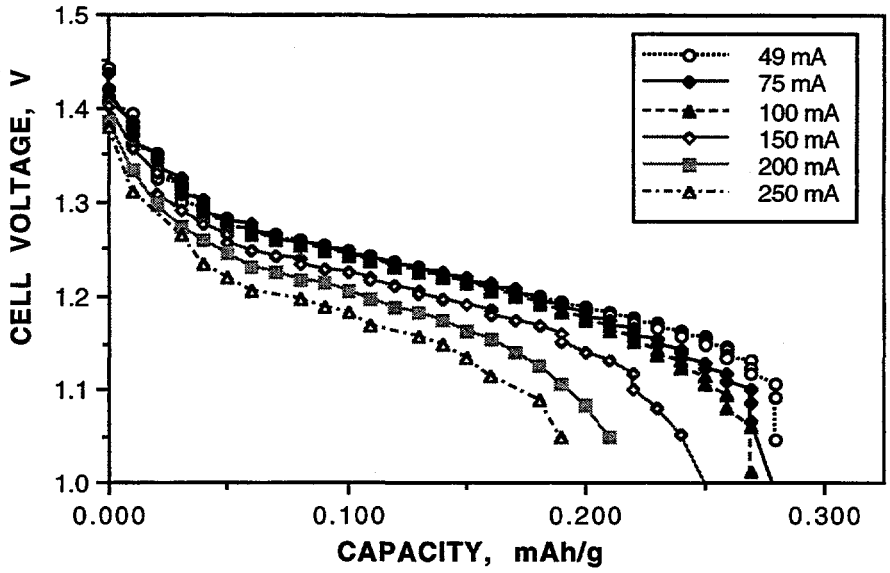

Fig. 11. Effects of discharge rates on cell voltage and capacity at 20°C. Curves are for discharges at various rates (48 to 480 mA) after charging for 165 min at a C/2 rate (120 mA) for a Ni/MH_x cell containing 927 mg of non-atomized R11 alloy powders in size range of 38-53 μm in diameter.

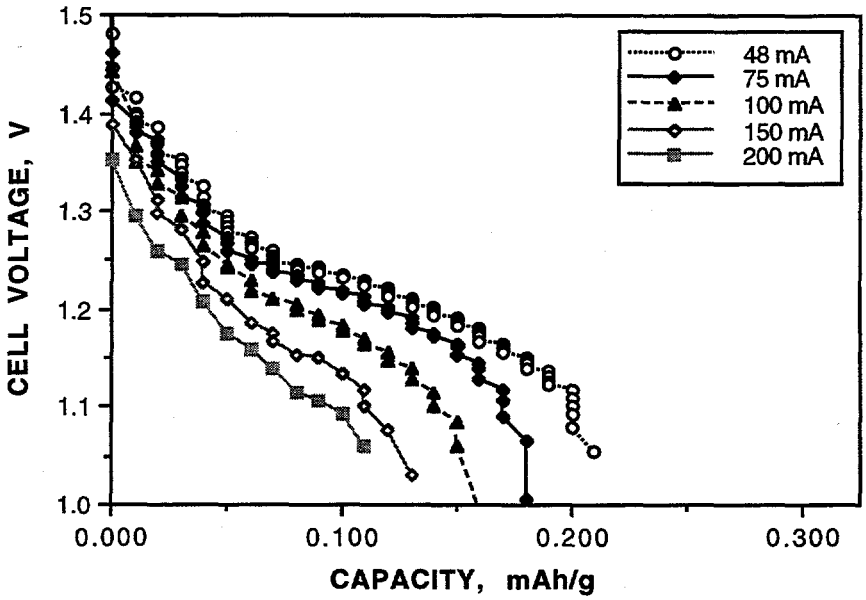

Fig. 12. Effects of discharge rates on cell voltage and capacity at 2°C. Curves are for discharges at various rates (48 to 200 mA) after charging for 165 min at a C/2 rate (120 mA) for a Ni/MH_x cell containing 890 mg of atomized R10 alloy powders in size range of 38-53 μm in diameter.

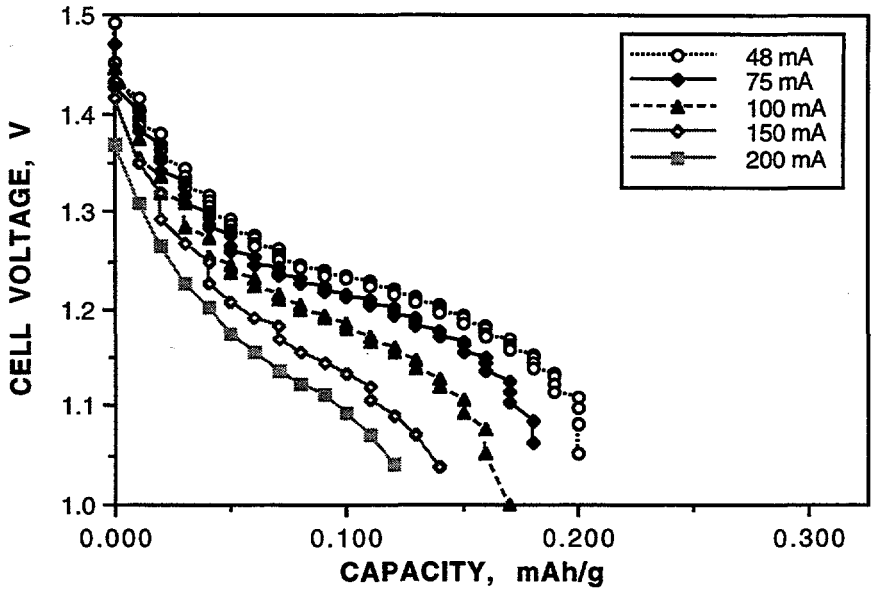

Fig. 13. Effects of discharge rates on cell voltage and capacity at 2°C. Curves are for discharges at various rates (48 to 200 mA) after charging for 165 min at a C/2 rate (120 mA) for a Ni/MH_x cell containing 843 mg of atomized R12 alloy powders in size range of 38-53 μm in diameter.

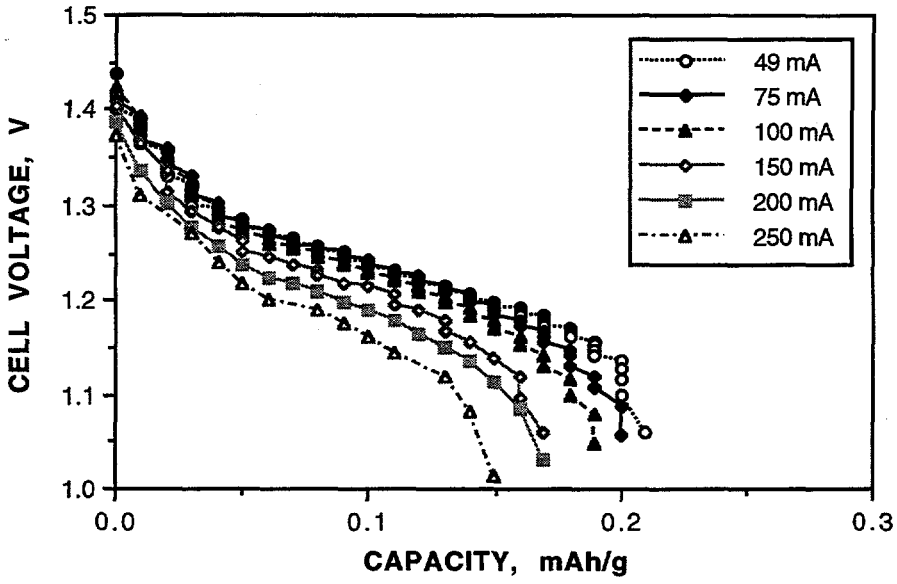

Fig. 14. Effects of discharge rates on cell voltage and capacity at 20°C. Curves are for discharges at various rates (48 to 480 mA) after charging for 165 min at a C/2 rate (120 mA) for a Ni/MH_x cell containing 890 mg of non-atomized R10 alloy powders in size range of 38-53 μm in diameter.

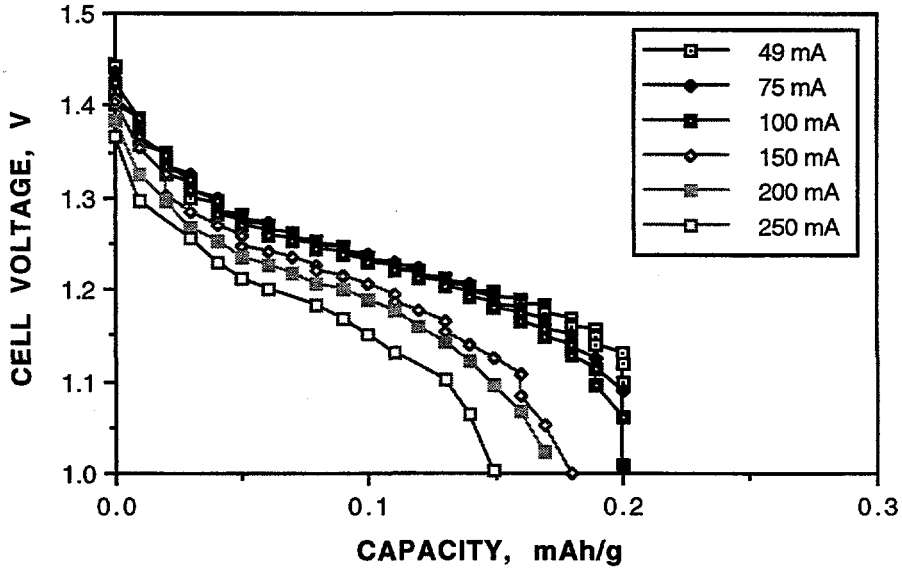

Fig. 15. Effects of discharge rates on cell voltage and capacity at 20°C. Curves are for discharges at various rates (48 to 480 mA) after charging for 165 min at a C/2 rate (120 mA) for a Ni/MH_x cell containing 843 mg of non-atomized R12 alloy powders in size range of 38-53 μm in diameter.

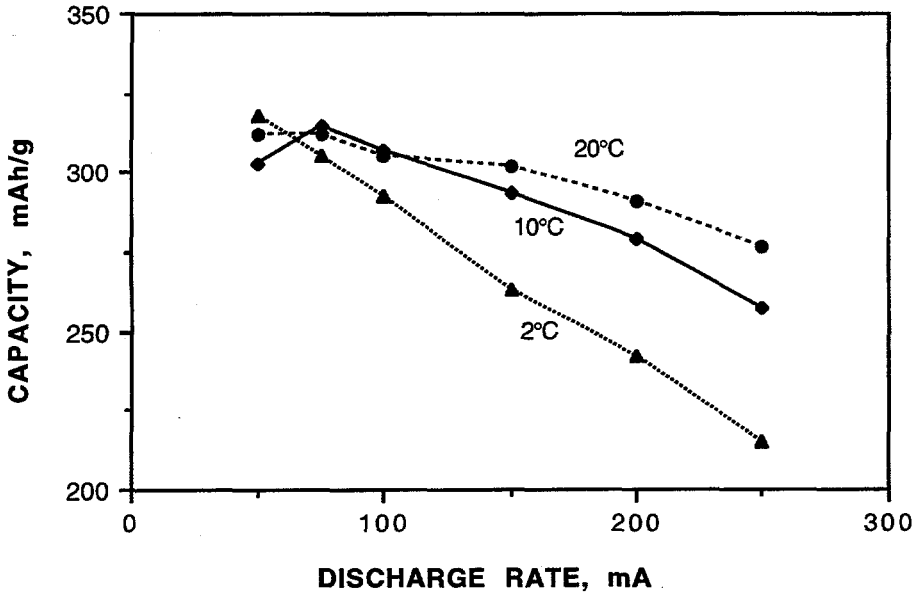

Fig. 16. Effects of temperature on discharge rate capability for a Ni/MH_x cell containing non-atomized R10 alloy powders.

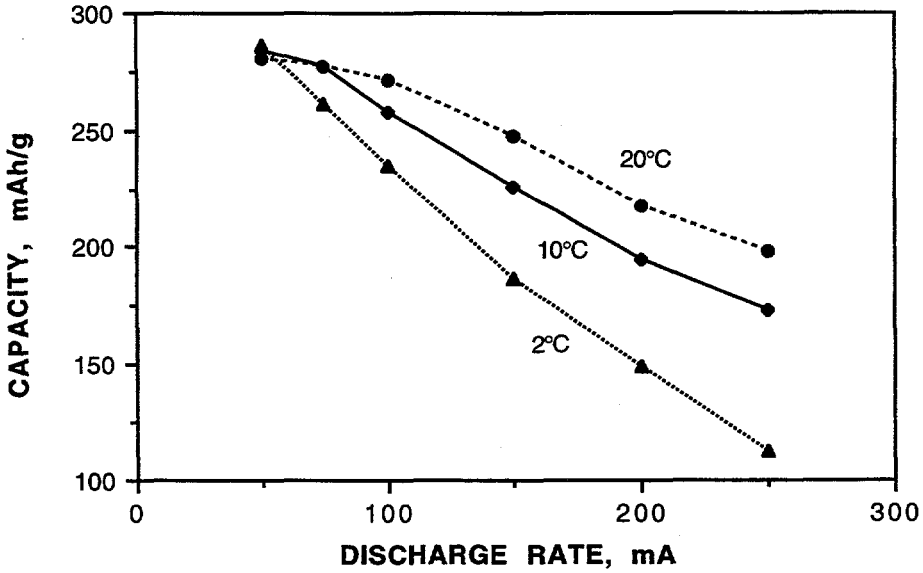

Fig. 17. Effects of temperature on discharge rate capability for a Ni/MH_x cell containing non-atomized R11 alloy powders.

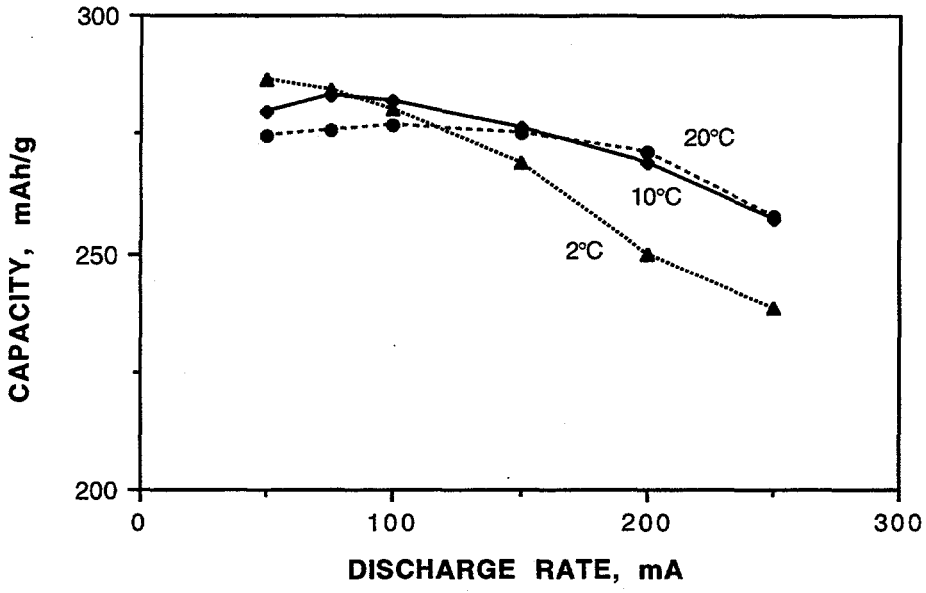

Fig. 18. Effects of temperature on discharge rate capability for a Ni/MH_x cell containing non-atomized R12 alloy powders.

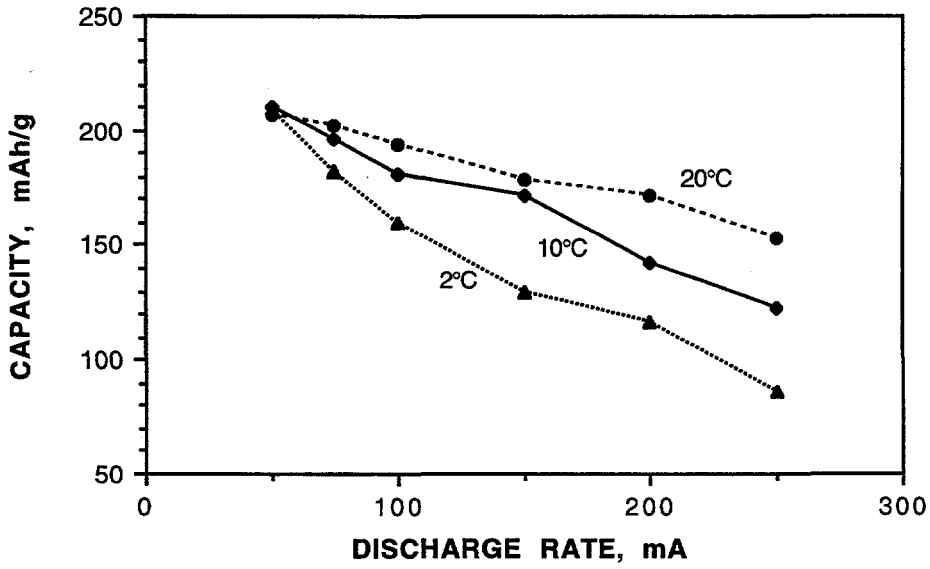

Fig. 19. Effects of temperature on discharge rate capability for a Ni/MH_x cell containing atomized R10 alloy powders.

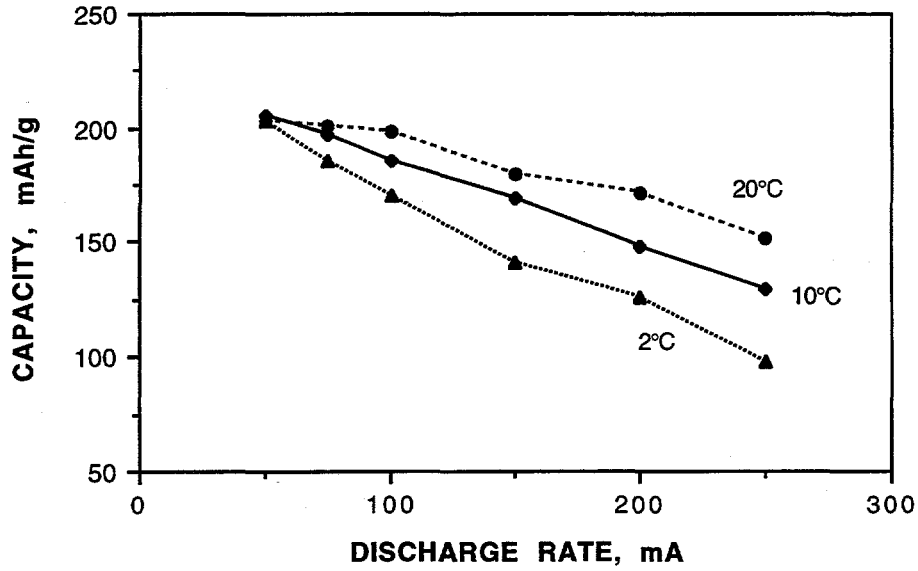

Fig. 20. Effects of temperature on discharge rate capability for a Ni/MH_x cell containing atomized R12 alloy powders.

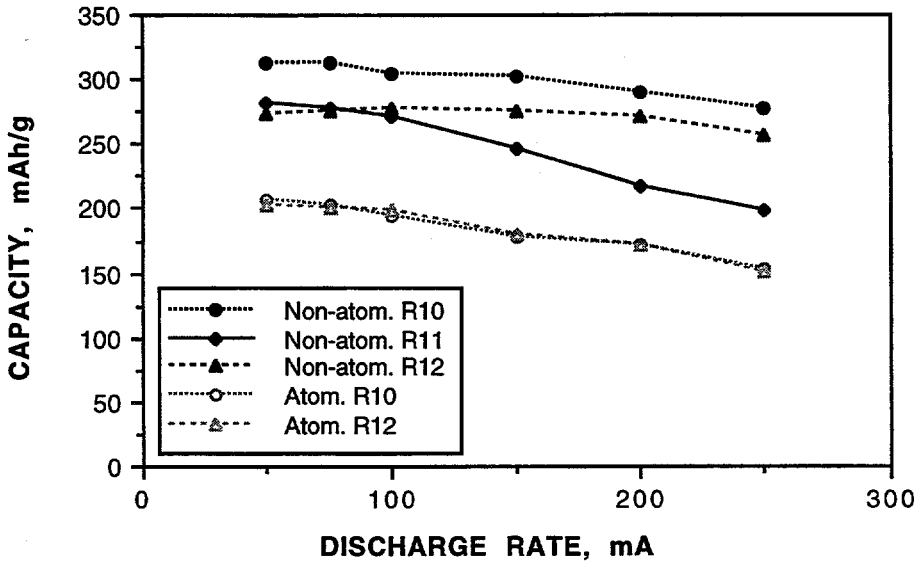

Fig. 21. Discharge rate capability for a Ni/MH_x cell containing various alloy powders at 20°C.

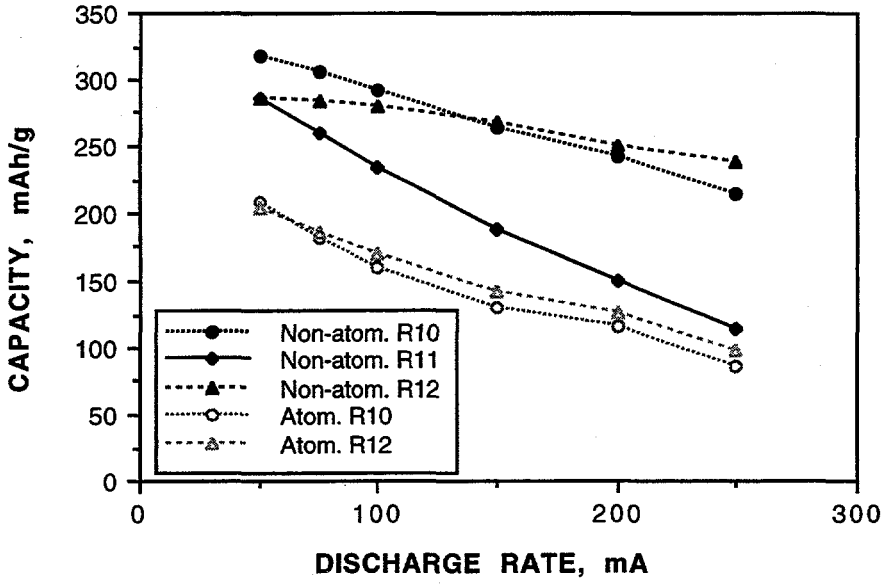

Fig. 22. Discharge rate capability for a Ni/MH_x cell containing various alloy powders at 2°C.

Effects of charge temperature on cell voltage and capacity were studied by charging cell at various temperatures followed by discharging at 20°C. Charge voltage curves of the Ni/H_x cells at various temperatures are shown in Figs. 23 and 24. Effects of charge temperature on cell discharge voltage and capacity for a cell containing R06 alloy are shown in Fig. 25. Charging temperatures above 30°C showed reduced capacity for this alloy. Effects of discharge temperature on cell voltage and capacity were studied by charging cell at 20°C followed by discharging at various temperatures. Results for a cell containing R06 alloy is shown in Fig. 26. Discharge temperatures between 10 and 40°C did not show a significant effect on capacity or voltage. However, both capacity and voltage were depressed noticeably when the cell was discharged at 0°C.

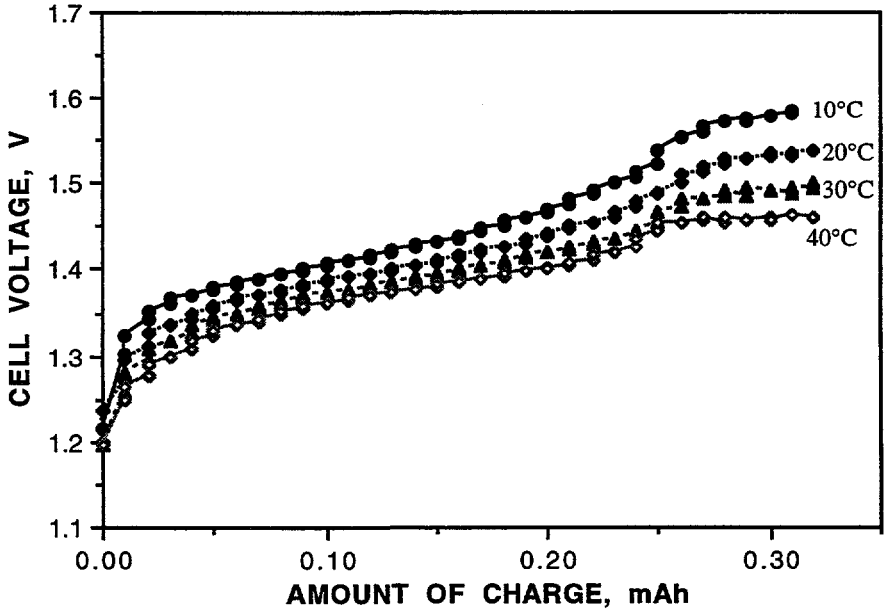

Fig. 23. Charge curves at various temperatures ranging from 10 to 40°C at a C/2 rate (120 mA) for a Ni/MH_x cell containing 861 mg of non-atomized R06 alloy powders in size range of 38-90 μm in diameter.

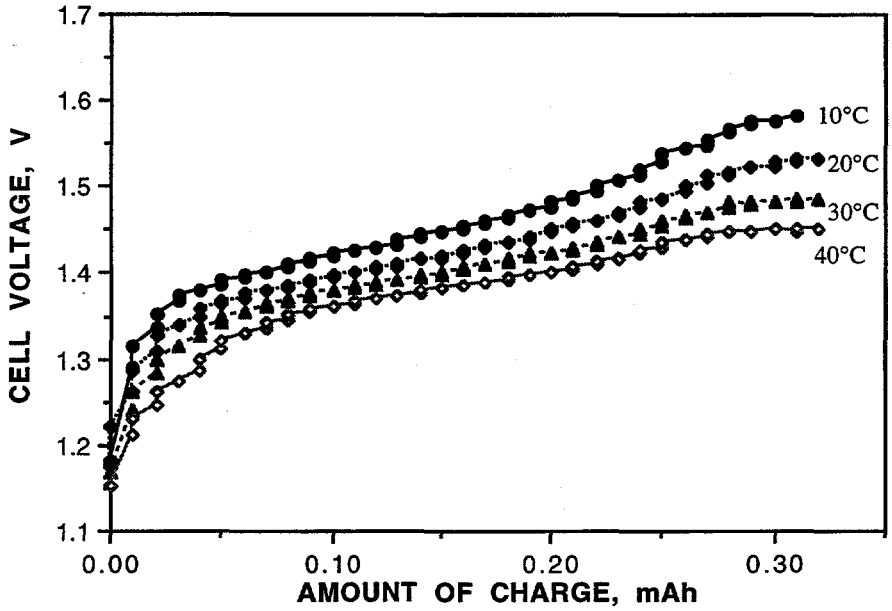

Fig. 24. Charge curves at various temperatures ranging from 10 to 40°C at a C/2 rate (120 mA) for a Ni/MH_x cell containing 861 mg of non-atomized R07 alloy powders in size range of 38-90 μm in diameter.

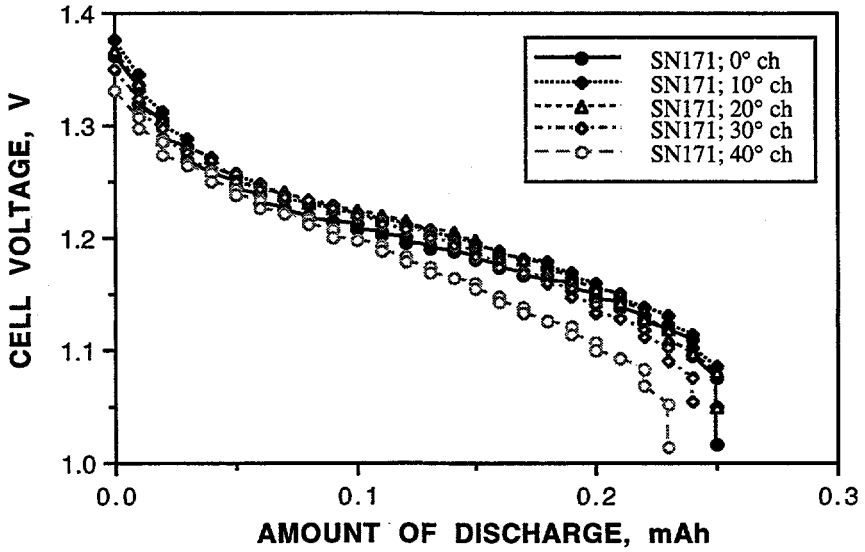

Fig. 25. Effects of charge temperature on cell voltage and capacity. Curves are for discharges at 20°C at a C/2 rate (120 mA) after charging 18 h at a C/10 rate or 165 min at a C/2 rate at various temperatures ranging from 10 to 40°C for a Ni/MH_x cell containing 861 mg of non-atomized R06 alloy powders in size range of 38-90 μm in diameter.

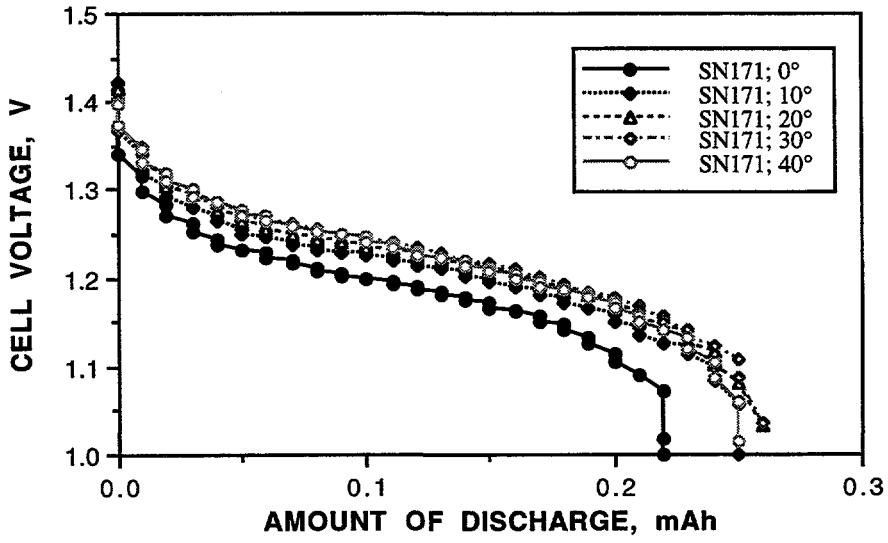

Fig. 26. Effects of discharge temperature on cell voltage and capacity. Curves are for discharges at various temperatures ranging from 0 to 40°C after charging at 20°C for 165 min at a C/2 rate (120 mA) for a Ni/MH_x cell 861 mg of containing non-atomized R06 alloy powders in size range of 38-90 μm in diameter.

Effects of Particle Size on Performance -- Powder size range for this study was rather limited because particle sizes bigger than approximately 100 μm (150 mesh) are not suitable for electrode fabrication. We have tested electrodes containing alloy powders in three different size ranges, i.e., below 38 μm, 38-63 μm, and 63-90 μm. The size below 38 μm did not give good capacities. Plots of capacity vs. number of cycles for electrodes containing two different powder sizes are shown in Fig 27 and 28. Rather surprisingly, the electrodes containing larger particles (63-90 μm) showed higher capacity and faster activation.

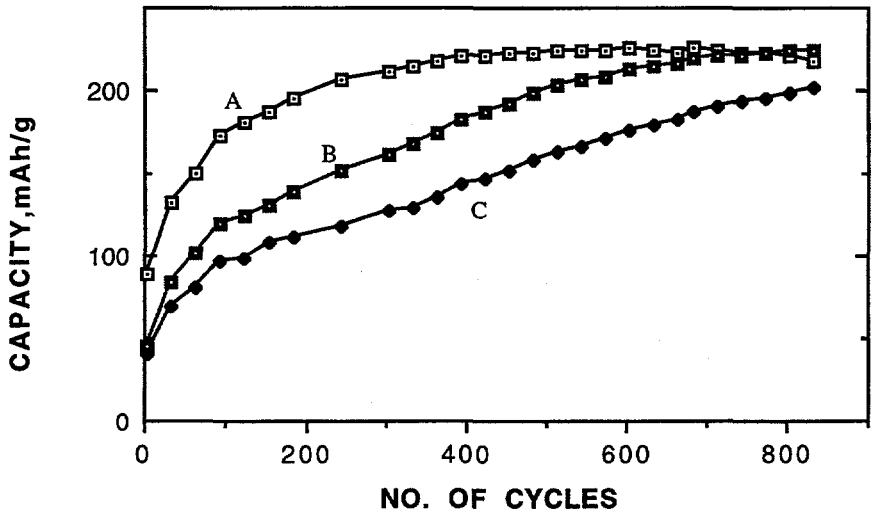

Fig. 27. Effects of particle size on capacity of electrodes made of atomized alloy powders of $La_{0.8}Ce_{0.2}Ni_{3.55}Co_{0.75}Mn_{0.4}Al_{0.3}$ in size range of (A) 63-90 μm and (B and C) 38-63 μm in diameter.

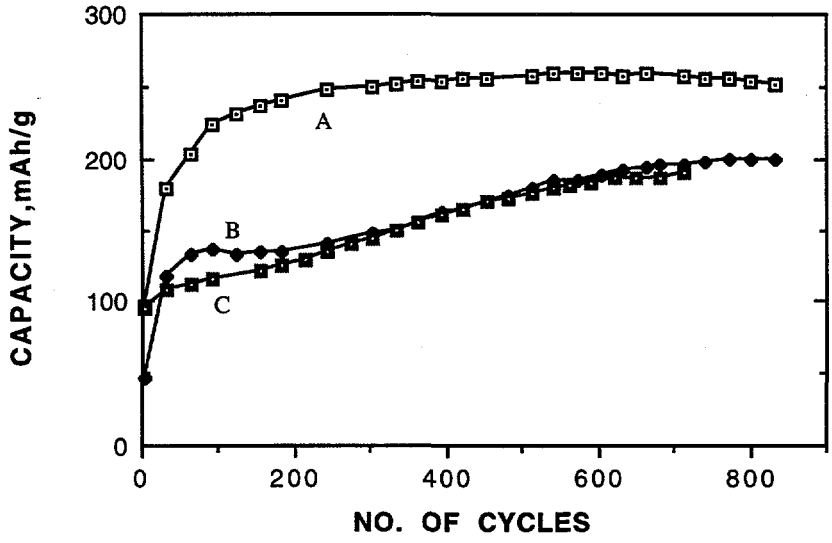

Fig. 28. Effects of particle size on capacity of electrodes made of atomized alloy powders of $La_{0.5}Ce_{0.5}Ni_{3.55}Co_{0.75}Mn_{0.4}Al_{0.3}$ in size range of (A) 63-90 μm and (B and C) 38-63 μm in diameter.

Effects of Atomization and Annealing on Cycle Life Performance -- We have studied the effects of atomization on the cycle life performance of the alloys. Comparative cycle life performances of non-atomized and atomized alloys are shown in Figs. 29 and 30. Electrodes with non-atomized powders activate faster and have a much higher initial capacity than the corresponding atomized alloys. However, a long term cycling (hundreds of cycles) showed that capacities of the non-atomized alloys are decreasing with cycling, while the atomized alloys showed a trend of increase in capacity.

We have also studied the effects of annealing of the atomized alloys on the alloy performance since we suspected that one of the possible reasons of the reduced capacity of atomized alloys compared with corresponding non-atomized alloys might be the highly non-crystalline nature of the atomized alloys. Comparative cycle life performances of non-annealed and annealed alloys are shown in Fig 31 and 32. (Cells containing the non-annealed alloy were stored under a 10-mA trickle charge condition for approximately three months for a period of time between initial characterization test and the long term cycle test.) For R10 alloy, the annealed alloy showed superior performance to the non-annealed, but the non-annealed alloy was superior for R12. This result for R12 alloy is contrary to that of the initial characterization test (see Table 6). The specific capacity of the non-annealed R12 alloy has improved greatly (from approximately 200 to 250 mAh/g) after the trickle charge period, while the annealed alloy did not improve.

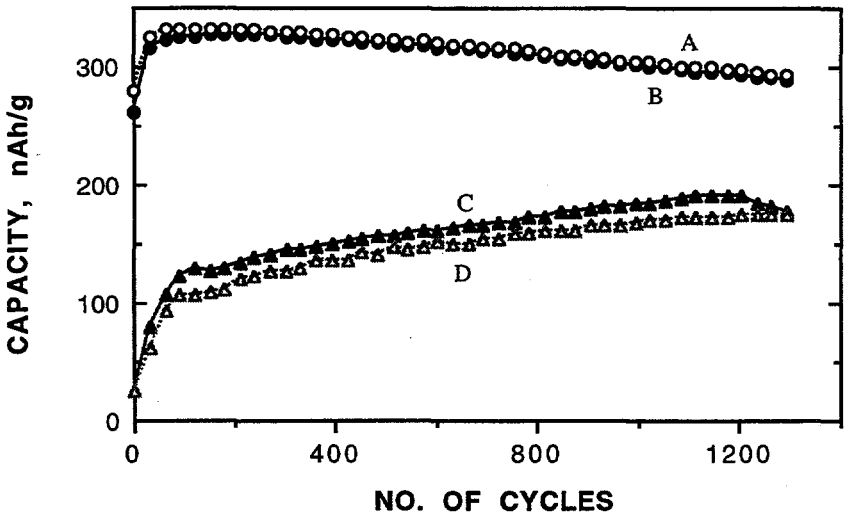

Fig. 29. Effects of atomized vs. non-atomized alloy powders on cycle life performance of MHx electrodes. Alloy: R06. (A) and (B) non-atomized powder of 63-90 μm. (C) and (D) atomized powder of 38-63 μm in diameter.

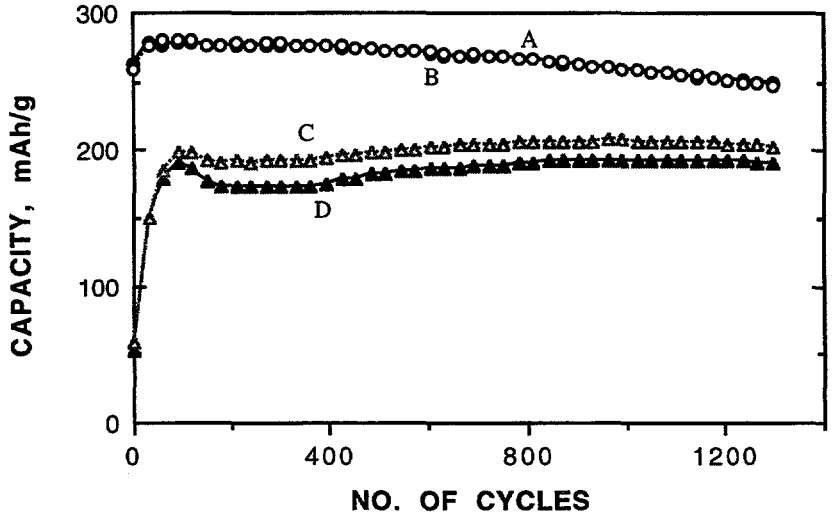

Fig. 30. Effects of atomized vs. non-atomized alloy powders on cycle life performance of MHx electrodes. Alloy: R07. (A) and (B) non-atomized powder of 63-90 μm. (C) and (D) atomized powder of 38-63 μm in diameter.

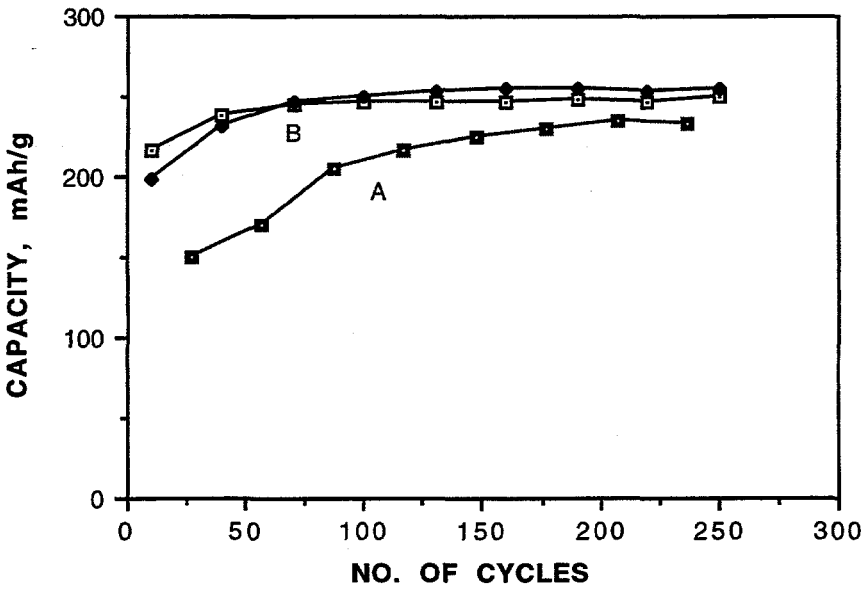

Fig. 31. Effects of annealing after atomization on cycle life performance of MHx electrodes. Alloy: R10. (A) non-annealed powder of 38-53 μm. (B) annealed powder of 38-90 μm.

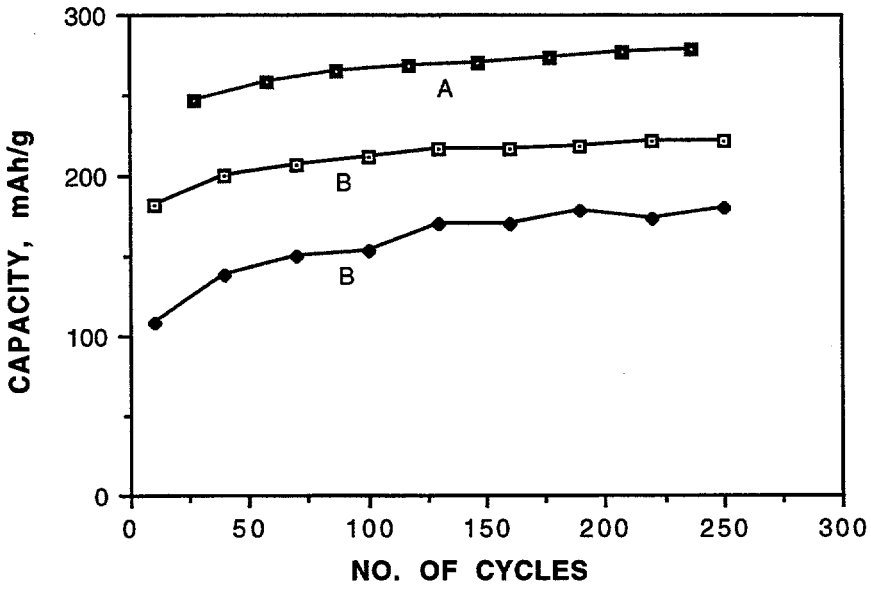

Fig. 32. Effects of annealing after atomization on cycle life performance of MHx electrodes. Alloy: R12. (A) non-annealed powder of 38-53 μm. (B) annealed powder of 38-90 μm.

6. ALLOY COATING

We have studied effects of nickel and copper surface coatings of alloy particles on the MH_X electrode performance. It has been reported that such coatings improve rate capability, utilization, and cycle life performance (11, 12, 13). The surface coating was carried out using a electroless coating technique. Ni-coating was carried out in an alkaline hypophosphite bath (Niklad™ 776A and 776H) at 75°C. Typical weight gain was 8-9% of original alloy weight. Cu-coating was carried out in an acidic copper sulfate bath. Copper coating was achieved by a displacement reaction by introducing alloy powder in a vigorously stirred solution of cupric sulfate solution containing copper in a quantity corresponding to approximately 5% of the alloy weight. The concentration of copper in the plating solution was approximately 0.5 M.

An SEM picture (5000x) of a cross-sectional view of a nickel coated mechanical powder is shown in Fig. 33. A partially peeled-off film (<1 μm thick) of the nickel coating is shown in the middle of the picture (indicated by an arrow). To confirm that the film is nickel, phosphorous (P) and nickel maps of EDAX/SEM were taken. High concentration of P in the film as shown in Fig. 34 is indicating that the film coated from a hypophosphite bath is made of a nickel film which generally contains P at server percentage level. The nickel map as shown in Fig 35 is also showing that the film is nickel. The nickel coated surface of atomized particles of R02 alloy is shown in Fig. 36.

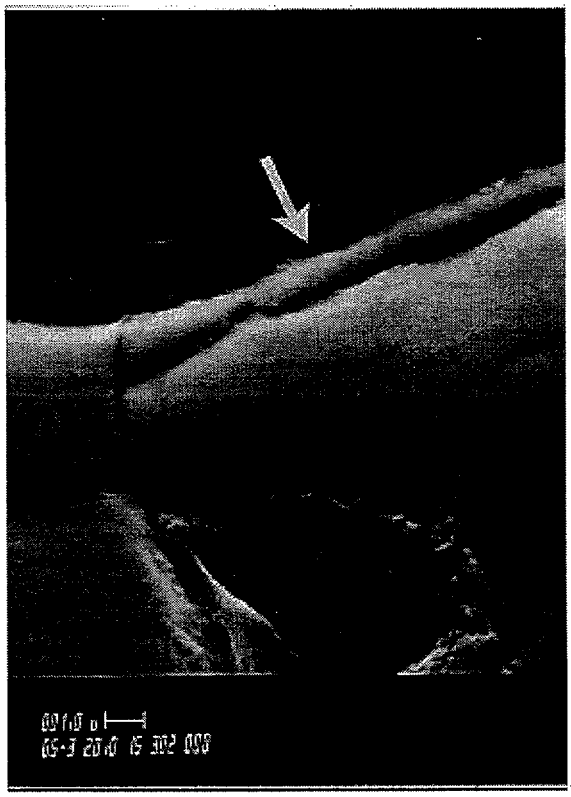

Fig. 33. SEM photograph (5000x) of an electroless Ni-coated particle of mechanical powder

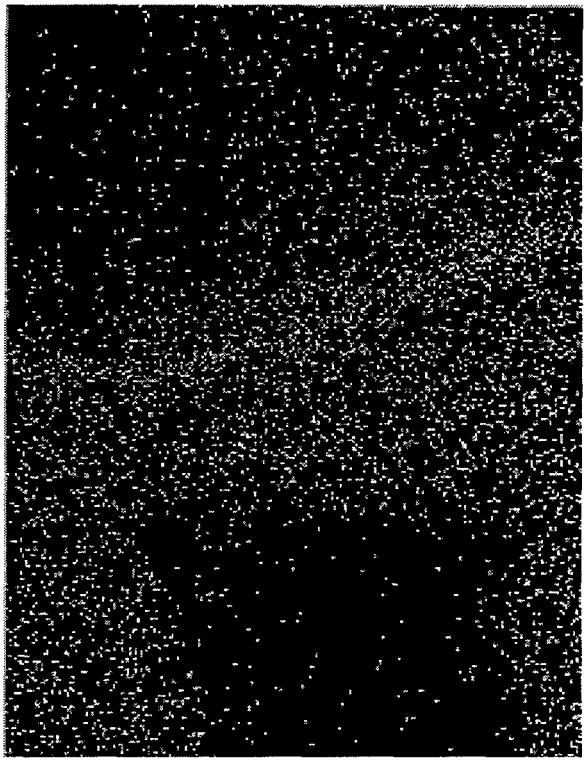

Fig. 34. Phosphorous map of EDAX/SEM photograph (5000x) of a Ni-coated particle of mechanical powder

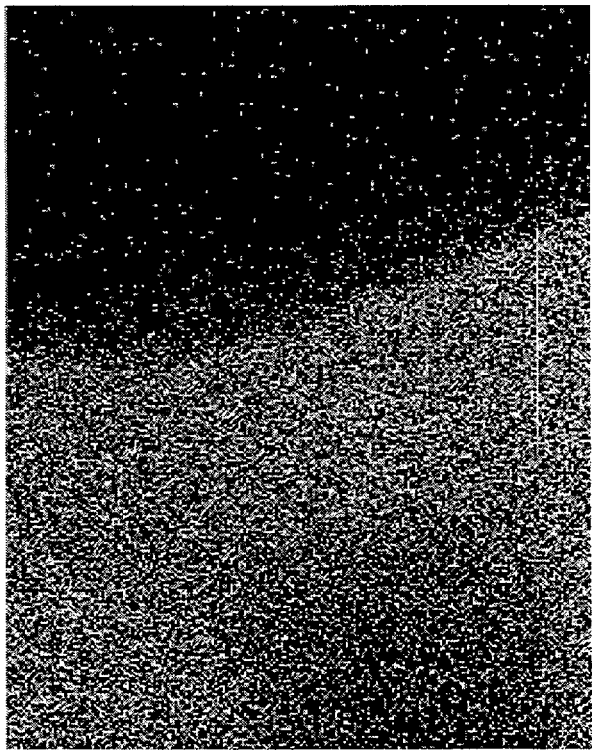

Fig. 35. Nickel map of EDAX/SEM photograph (5000x) of a Ni-coated particle of mechanical powder

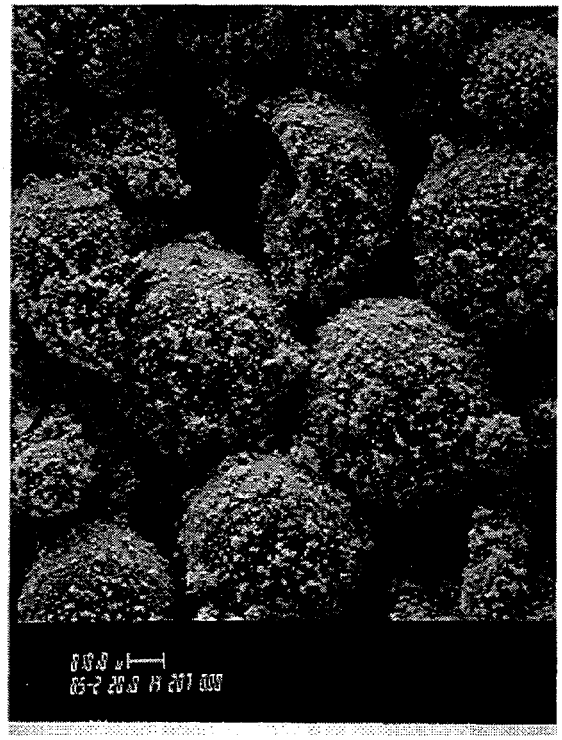

Fig. 36. SEM photograph (500x) of a Ni-coated atomized particles of R02 alloy in the particle size range of 38 to 63 μm.

Performance of Ni- and Cu-coated Alloys -- We have studied effects of the Ni- and Cu-coatings on the alloy performance. Charge and discharge voltage curves of Ni/MH_x cells containing alloys without and with the Ni-coating are shown in Fig. 37 for non-atomized alloys and in Fig. 38 and 39 for atomized alloys. Similar voltage curves for atomized alloys without and with the Cu-coating are shown in Fig. 40. Both Ni- and Cu-coatings reduced the electrode polarization drastically thus improving the electrode rate capability and the electrochemical utilization of the alloys was also improved drastically. Effects of the Ni- and Cu-coatings on the cycle life performances of the alloys are shown in Figs. 41 and 42. Ni-coated alloys showed faster activation than corresponding un-coated alloys. However after long cycling their performances appear to converge to a similar specific capacity value as indicated in Fig 41.

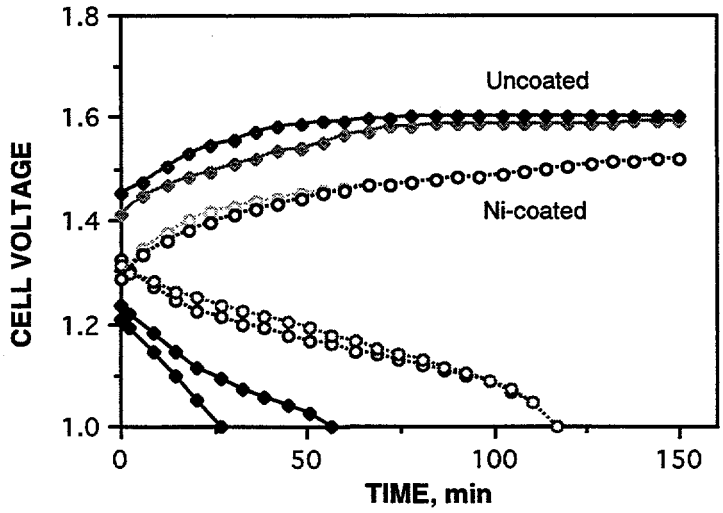

Fig. 37. Charge and discharge voltage curves at 100 mA of Ni/MH_x cells made of un-coated and Ni-coated non-atomized E932 alloy electrodes. Alloy powder size was 30-38 μm in diameter.

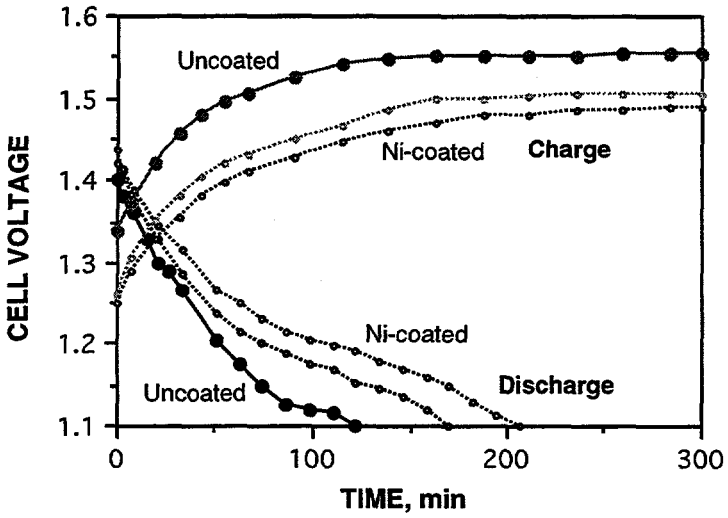

Fig. 38. Charge (at 80 mA) and discharge (at 70 mA) voltage curves of Ni/MHx cells made of bare and Ni-coated atomized E932 alloy electrodes. Alloy powder size was 38-75 μm in diameter.

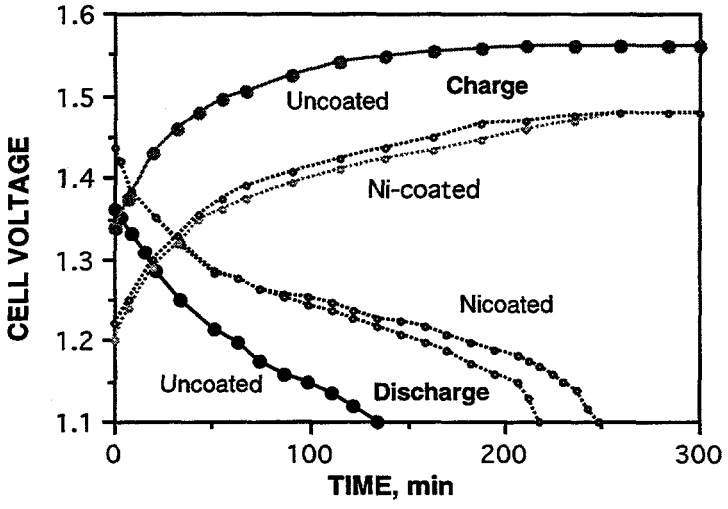

Fig. 39. Charge (at 80 mA) and discharge (at 70 mA) voltage curves of Ni/MHx cells made of hydride electrodes containing un-coated and Ni-coated atomized E931 alloy. Alloy powder size was 38-75 μm in diameter.

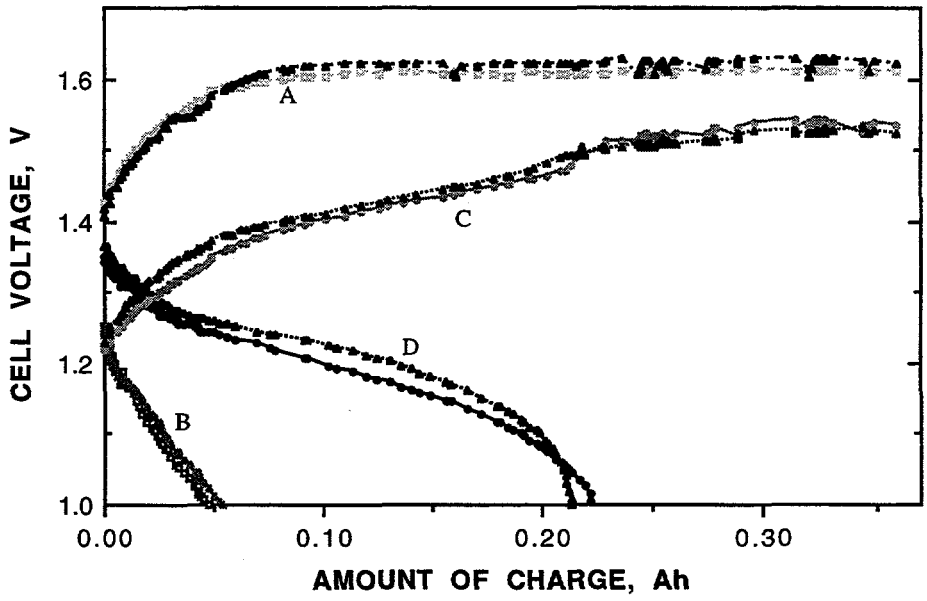

Fig. 40. Charge (at 70 mA) and discharge (at 75 mA) voltage curves of Ni/MHx cells made of hydride electrodes containing un-coated and Cu-coated atomized R06 alloys in particle size 63-90 μm in diameter. (A) Charge curves of duplicate cells for un-coated alloy (0.868 and 0.965 g, respectively). (B) Discharge curves of these cells. (C) Charge curves of duplicate cells for Cu-coated alloy (0.858 and 0.915 g, respectively). (D) Discharge curves of these cells.

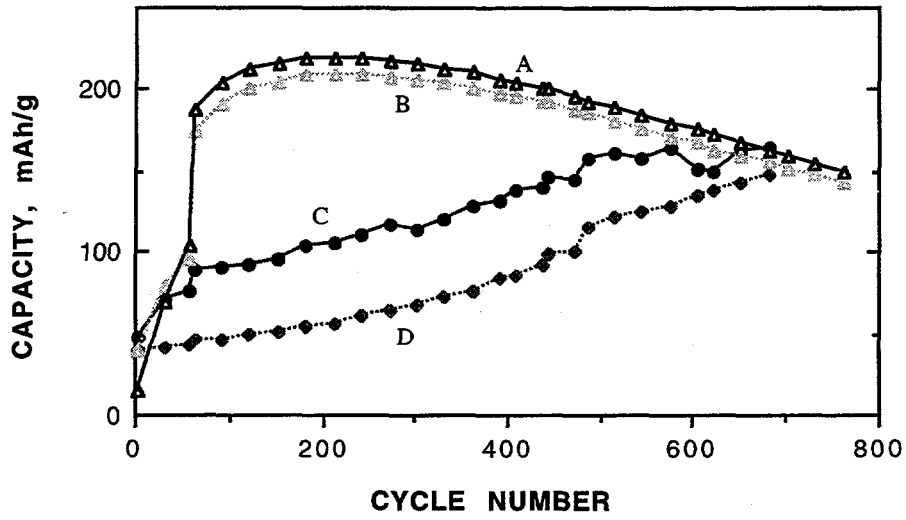

Fig. 41. Effects of Ni-coating on capacity of electrodes made of atomized E932 alloy powders. (A) and (B) Ni-coated; particle size 38-75 μm in diameter. (C) un-coated; particle size 38-75 μm in diameter. (D) un-coated; particle size smaller than 38 μm in diameter.

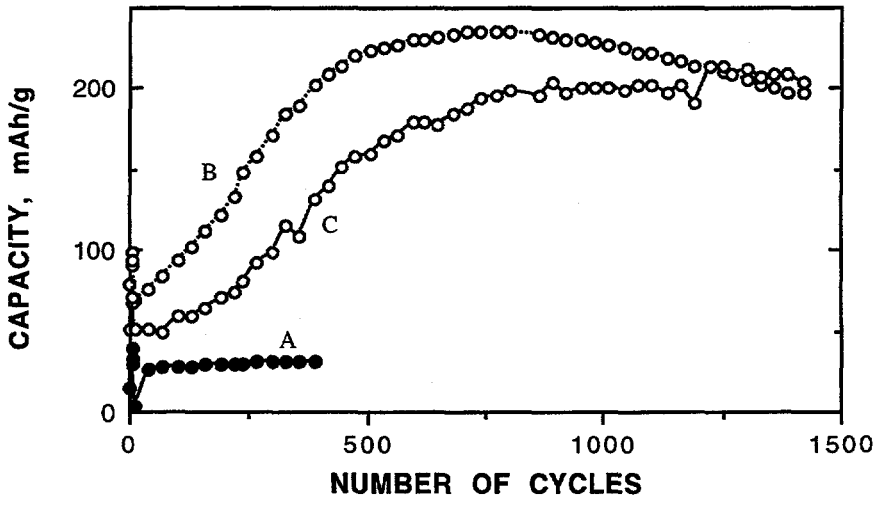

Fig. 42. Effects of Ni-coating on capacity of electrodes made of atomized alloy powders of R05 in particle size 63-90 μm in diameter. (A) not coated. (B) and (C) Ni-coated.

7. PHYSICAL CHANGES OF ALLOYS BY CYCLING

In order to study physical changes of the alloys with the electrochemical cycling in a Ni/MH_x cell, we have separated alloy particles from cycled electrode by dissolving the polymer used for the bonding of the active material. The physical integrity of these particles after various number of cycles is shown by SEM pictures in Fig. 43-45. The mechanical degradation of R02 alloy particles after 387 cycles was minimal as shown in Fig. 43. After 862 cycles, R01 alloy particles were slightly degraded as shown in Fig. 44. The degradation of Ni-coated R02 alloy particles after 742 cycles was rather pronounced in Fig. 45 indicating that the degradation process might have been accelerated by the nickel coating.

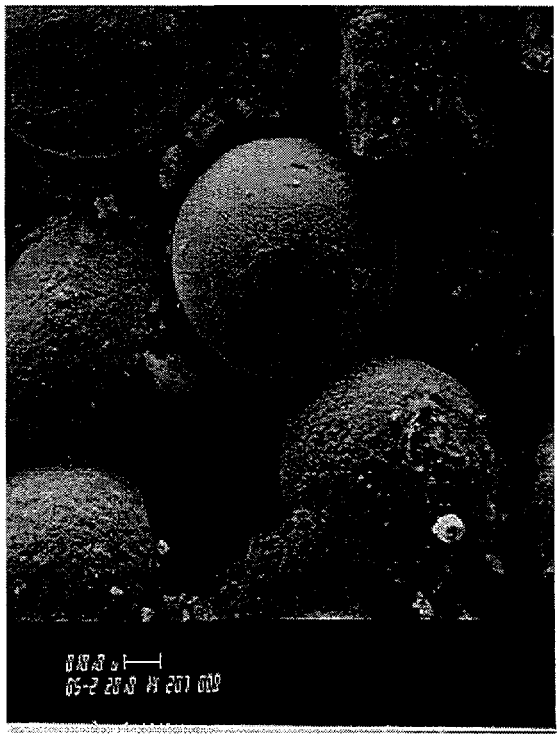

Fig. 43. SEM picture of R02 alloy in particle size 63-90 μm in diameter after 387 cycles.

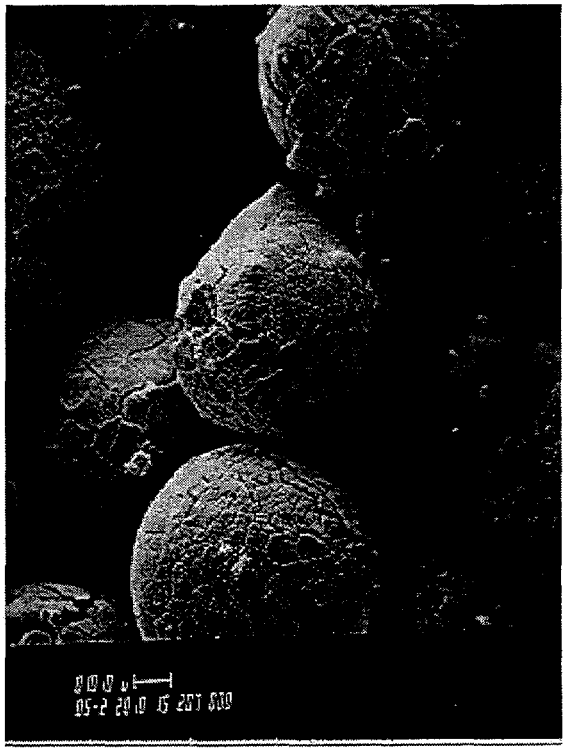

Fig. 44. SEM picture of R01 alloy in particle size 63-90 μm in diameter after 862 cycles.

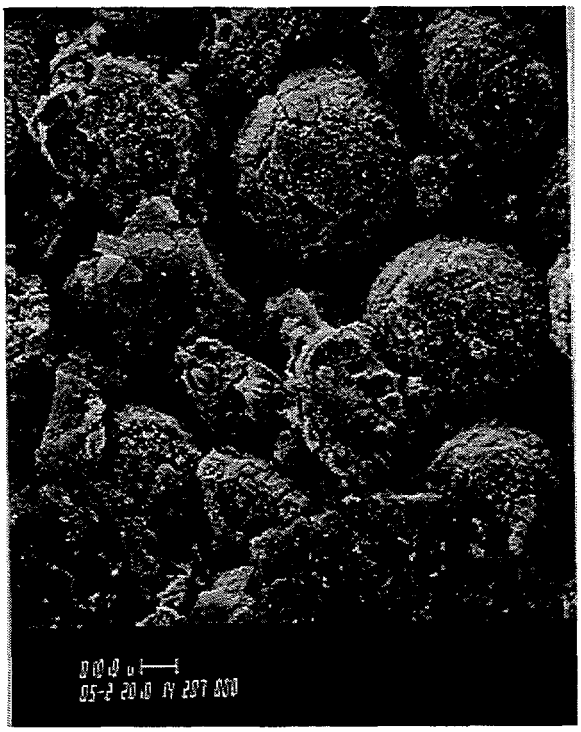

Fig. 45. SEM picture of Ni-coated R02 alloy in particle size 63-90 μm in diameter after 742 cycles.

8. SUMMARY

We have studied inert gas atomization technique using several metal hydride alloys which are attractive for a Ni/MH_x cell. Atomization of the alloys was demonstrated successfully in a small production scale (up to a batch-size of several kilograms). The relative performances of the atomized and corresponding non-atomized alloys for electrode material in a Ni/MH_x cell were investigated extensively. The study included effects of charge-discharge rates, temperature, and particle size on cell voltage (polarization) and specific capacity. Results show that the specific capacity of the present atomized alloys was appreciably smaller than that of the corresponding non-atomized powder, especially for initial cycles. Full activation of the atomized alloys often took several hundreds of cycles. Even after full activation, the specific capacity of the atomized alloys was smaller than that of the corresponding non-atomized alloy. However, no appreciable difference in discharge rate capability was observed with R10 and R12 alloys.

Results of chemical analyses of the metallic composition were indistinguishable between the atomized and non-atomized alloys. However, the oxygen contents of the atomized alloys were always higher by a factor of 3 or more than those of the non-atomized alloys. We suspect that the high oxygen content might be a factor for the low specific capacity of the atomized alloys. We have also studied the effect of annealing of the atomized alloys at 1100°C, since we suspected that a lack of crystallinity might be another factor for the low specific capacity of the atomized alloys. The annealing improved the capacity, but the alloy capacity is still smaller than that of the non-atomized alloy.

Effects of Ni- and Cu coating on the alloy performance were studied after coating the powder alloys using an electroless coating technique. Coatings of both metals noticeably improved the electrode rate capability for all alloy samples studied. Especially, the improvement in the electrode polarization for atomized alloys was tremendous. However, the coating did not appear to improve their cycle life. Spherical geometry of the atomized powder allowed us a means of a direct observation of the mechanism and rate of physical changes of the alloy particles. Present results of a preliminary investigation are not conclusive to determine the possible merits of the atomization technique, even though overall performances of the non-atomized alloy were superior to those of the atomized alloy. Further studies are needed, especially to reduce the oxygen contents in the atomized alloys, to explore possible merits of atomization technique, e.g., possible improved life without sacrificing the specific capacity and the rate capability.

References

1. G. G. Libowitz, "An introduction to metallic hydrides and their applications", Proc. Sym. "Hydrogen Storage Materials, Batteries, and Electrochemistry" Ed by D. Corrigan and S. Srinivasan, Proc. Vol. 92-5, Electrochemical Soc., Pennington, NJ, p. 3.

2. T. Sakai et al, "Rechargeable hydrogen batteries using rare-earth-based hydrogen storage alloys," J. Alloys and Compounds, 180, 37-54 (1992).

3. K. Suzuki, "A structural study of the solid state vitrification of metals and oxides by ball milling," J. Non-Crystalline Solids, 112, 23 (1989).

4. T. Ikeya et al, "Modification by mechanical treatment of metal hydride for the anode of a Ni/MH secondary battery", Electrochem. Soc. Fall Meeting, Toronto, Canada, Oct. 11-16, 1992, Abs. No. 65.

5. T. Ikeya et al, "Mechanical process for enhancing metal hydride for the anode of a Ni-MH secondary battery," J. Electrochem. Soc., 140, 3082 (1993).

6. T. Sakai et al, "Rare-earth-based alloy electrodes for Ni/MHx battery," J. Less-Common Metals, 172-174, 1175-84 (1991).

7. T. Murada and K. Koshiro, "Hydrogen absorbing electrode characteristics of Ti-Ni alloy powder prepared by gas atomization process," G. S. New Tech. Rep., 50(1), 21-29 (1991).

8. H. Hasebe, Europe Patent, 420,669, April 4, 1991.

9. H. S. Lim, D. F. Pickett, J. F. Stockel, and J. J. Smithrick, "Advanced nickel-metal hydride cell development at Hughes - A joint work with U. S. government," Conf. on NASA Centers for Commercialization & Development of Space, Albuquerque, NM, Jan. 8-12, 1995; Proc. 10th Annual Battery Conference on Applications and Advances, January 10-13, 1995, Long Beach, CA. p. 65.

10. H. S. Lim, "Status of advanced nickel-metal hydride cell development" Space Battery Workshop, Albuquerque, NM, April. 17-19, 1995.

11. C. Iwakura et al, "Surface modification of metal hydride negative electrodes and their charge/discharge performance," J. Power Sources, 38, 335-343 (1992).

12. T. Sakai et al, "Ni/MHx battery using microencapsulated alloys," J. Less-Common Metals, 172-174, 1194-1204 (1991)

13. T. Sakai et al, J. Electrochem. Soc., 134, 558 (1987).

14. H. S. Lim, unpublished results from "Hydride Research" program (Aug. 92 - Aug. 95) supported by Office of Research and Development (Contract No. 92F-142400-000), Hughes Electronics, and Center for Space Power.

Publications

1. H. S. Lim, D. F. Pickett, J. F. Stockel, and J. J. Smithrick, "Advanced nickel-metal hydride cell development at Hughes - A joint work with U.S. government," Conf. on NASA Centers for Commercialization & Development of Space, Albuquerque, NM, Jan. 8-12, 1995; Proc. 10th Annual Battery Conference on Applications and Advances, Jan 10-13, 1995, Long Beach, CA. p. 65.

2. H. S. Lim, "Status of advanced nickel-metal hydride cell development" Space Battery Workshop, Albuquerque, NM, April. 17-19, 1995.

3. H. S. Lim and G. R. Zelter, "Characteristics of nickel-metal hydride cells containing metal hydride alloys prepared by an atomization technique," to be published.

4. H. S. Lim and G. R. Zelter, "Effects of Ni- and Cu-coating of hydride alloys on the electrode reactions of metal hydride electrodes" to be published.